HHS Public Access

Author manuscript

Cell Rep. Author manuscript; available in PMC 2018 November 29.

Published in final edited form as:

Cell Rep. 2018 October 16; 25(3): 571–584.e5. doi:10.1016/j.celrep.2018.09.049.

Complementary Wnt Sources Regulate Lymphatic Vascular Development via PROX1-Dependent Wnt/β-Catenin Signaling

Boksik Cha[1], **Xin Geng**[1], **Md. Riaj Mahamud**[1,2], **Jenny Y. Zhang**[3], **Lijuan Chen**[1], **Wantae Kim**[4], **Eek-hoon Jho**[5], **Yeunhee Kim**[6], **Dongwon Choi**[7], **J. Brandon Dixon**[8], **Hong Chen**[9], **Young-Kwon Hong**[7], **Lorin Olson**[1,2], **Tae Hoon Kim**[6], **Bradley J. Merrill**[3], **Michael J. Davis**[10], and **R. Sathish Srinivasan**[1,2,11,*]

[1]Cardiovascular Biology Research Program, Oklahoma Medical Research Foundation, Oklahoma City, OK, USA

[2]Department of Cell Biology, University of Oklahoma Health Sciences Center, Oklahoma City, OK, USA

[3]Department of Biochemistry and Molecular Genetics, University of Illinois, Chicago, IL, USA

[4]Rare Disease Research Center, Korea Research Institute of Bioscience and Biotechnology (KRIBB), Deajeon, Korea

[5]Department of Life Science, University of Seoul, Seoul, Korea

[6]Department of Biological Sciences and Center for Systems Biology, The University of Texas at Dallas, Richardson, TX, USA

[7]Keck School of Medicine, University of Southern California, Los Angeles, CA, USA

[8]Parker H. Petit Institute for Bioengineering and Bioscience, Georgia Institute of Technology, Atlanta, GA, USA

[9]Vascular Biology Program, Boston Children's Hospital, Boston, MA, USA

[10]Department of Medical Pharmacology and Physiology, University of Missouri, Columbia, MO, USA

[11]Lead Contact

SUMMARY

*Correspondence: sathish-srinivasan@omrf.org.

AUTHOR CONTRIBUTIONS

B.C., X.G., M.R.M., L.C., Y.K., L.O., T.H.K., M.J.D., and R.S.S. performed the experiments. J.Y.Z., W.K., E.-h.J., D.C., J.B.D., H.C., Y.-K.H., and B.J.M. provided critical reagents. B.C. and R.S.S. designed the experiments and wrote the manuscript. All authors provided input regarding design of the experiments and writing of the manuscript.

DECLARATION OF INTERESTS

The authors declare no competing interests.

SUPPLEMENTAL INFORMATION

Supplemental Information includes eight figures and one table and can be found with this article online at https://doi.org/10.1016/j.celrep.2018.09.049.

Wnt/β-catenin signaling is necessary for lymphatic vascular development. Oscillatory shear stress (OSS) enhances Wnt/β-catenin signaling in cultured lymphatic endothelial cells (LECs) to induce expression of the lymphedema-associated transcription factors *GATA2* and *FOXC2*. However, the mechanisms by which OSS regulates Wnt/β-catenin signaling and *GATA2* and *FOXC2* expression are unknown. We show that OSS activates autocrine Wnt/β-catenin signaling in LECs *in vitro*. Tissue-specific deletion of Wntless, which is required for the secretion of Wnt ligands, reveals that LECs and vascular smooth muscle cells are complementary sources of Wnt ligands that regulate lymphatic vascular development *in vivo*. Further, the LEC master transcription factor PROX1 forms a complex with β-catenin and the TCF/LEF transcription factor TCF7L1 to enhance Wnt/β-catenin signaling and promote *FOXC2* and *GATA2* expression in LECs. Thus, our work defines Wnt sources, reveals that PROX1 directs cell fate by acting as a Wnt signaling component, and dissects the mechanisms of PROX1 and Wnt synergy.

In Brief

Cha et al. demonstrate that lymphatic vascular development is regulated by Wnt ligands secreted by lymphatic endothelial cells (LECs) and vascular smooth muscle cells. Oscillatory shear stress regulates Wnt secretion from LECs. PROX1 interacts with β-catenin and TCF7L1 to regulate Wnt signaling and promote the expression of FOXC2 and GATA2.

Graphical Abstract

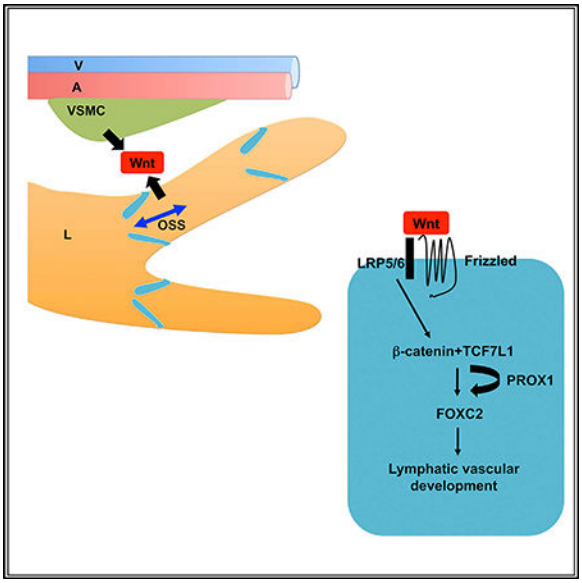

INTRODUCTION

The mammalian lymphatic vasculature transports lymph via lymphatic vessels. Intraluminal lymphatic valves (LVs) within collecting lymphatic vessels ensure the unidirectional flow of lymph toward the junction of the thoracic duct and the jugular and subclavian veins, where the lymphovenous valves (LVVs) regulate lymph return to the blood circulation (Geng et al., 2017; Tammela and Alitalo, 2010). Defects in lymphatic vessels or valves can cause

lymphedema, obesity, fibrosis, high blood pressure, and angiosarcoma (Harvey et al., 2005; Machnik et al., 2009; Ruocco et al., 2002). Although palliative approaches such as massages and compression bandages are available, therapeutic approaches to cure lymphedema currently do not exist. Identifying the genetic regulators of the lymphatic vasculature might illuminate strategies to repair damaged vessels and/or valves.

We recently demonstrated the stepwise development of LVVs in mouse embryos (Geng et al., 2016). Differentiation of LVV-forming endothelial cells (LVV-ECs) occurs at embryonic day 12.0 (E12.0), concomitant with increased expression of the transcription factors PROX1, FOXC2, and GATA2 in a subset of ECs at the junction of the jugular and subclavian veins. Integrin-α5 and Integrin-α9 are also strongly expressed in LVV-ECs at this stage (Geng et al., 2016; Turner et al., 2014). Newly differentiated LVV-ECs delaminate from the venous wall in the luminal direction (Geng et al., 2016). Within 12 hr, LVV-ECs reaggregate, invaginate into the vein, and undergo profound elongation perpendicular to the direction of blood flow to form LVVs.

Similar to LVV-ECs, LV-forming ECs (LV-ECs) differentiate with the upregulation of PROX1, FOXC2, and GATA2 in a subset of lymphatic endothelial cells (LECs) within collecting lymphatic vessels (Bazigou et al., 2009; Norrmén et al., 2009; Sabine et al., 2012). Expression of Integrin-a9 is then upregulated in LV-ECs, which undergo circumferential localization along the rim of the lymphatic vessel (Bazigou et al., 2009; Tatin et al., 2013). Next, LV-ECs protrude into the lumen of the vessel, forming a circular shelf. Finally, the cells at the inner edge of the circular shelf elongate to touch the vessel wall, forming a dome-shaped bicuspid LV.

PROX1, FOXC2, and GATA2 are essential for the differentiation of valvular ECs. Haploinsufficiency of *Prox1* abolishes LVV-EC differentiation (Geng et al., 2016; Srinivasan and Oliver, 2011), and LV development occurs only in a subset of $Prox1^{+/-}$ pups (Johnson et al., 2008). Valvular EC differentiation does not occur in $Foxc2^{+/-}$ embryos (Petrova et al., 2004). $Foxc2^{+/-}$ embryos lack 50%, if not all, LVVs (Geng et al., 2016) and display reduced numbers of LVs in the skin (but not in the mesentery) (Kanady et al., 2015). LVVs and LVs are absent in mice lacking GATA2 (Geng et al., 2016; Kazenwadel et al., 2015).

Valves develop in locations that are exposed to oscillatory shear stress (OSS). Hence, OSS has been proposed as an upstream regulator of valvular EC differentiation in zebrafish and in mammals (Sabine et al., 2012; Vermot et al., 2009). Consistent with this model, OSS-treated LECs show enhanced expression of *Foxc2* and *GATA2*, transcription factors that regulate valve development (Kazenwadel et al., 2015; Sabine et al., 2012; Sweet et al., 2015). We recently showed that Wnt/β-catenin signaling is also necessary for the development of valves (Cha et al., 2016). Furthermore, we showed that OSS activates Wnt/β-catenin signaling in LECs and that OSS-mediated expression of *GATA2* and *FOXC2* is dependent on Wnt/β-catenin signaling (Cha et al., 2016). However, important questions regarding Wnt/β-catenin signaling in lymphatic development remain. How OSS activates Wnt/β-catenin signaling is unknown. The relationship between the lymphatic master regulator PROX1 and OSS is not fully defined. PROX1 enhances Wnt/β-catenin signaling in cancer cell lines (Choi et al., 2016; Liu et al., 2015). However, the mechanism by which PROX1 enhances

Wnt/β-catenin signaling and whether the PROX1 and Wnt axis is relevant for *FOXC2* and *GATA2* expression in the lymphatic vasculature remains unknown.

RESULTS

OSS Activates Autocrine Wnt/β-Catenin Signaling in LECs In Vitro

Wnt/β-catenin signaling is activated upon the interaction of canonical Wnt ligands with Frizzled receptors and LRP5 and 6 (LRP5/6) co-receptors (Logan and Nusse, 2004). Wnt ligands induce the phosphorylation of LRP5/6 (Niehrs and Shen, 2010). We observed increased phosphorylation of LRP6 in primary human LECs (HLECs) exposed to OSS, suggesting that Wnt ligands are involved in OSS-mediated activation of Wnt/β-catenin signaling (Figure 1A). To evaluate whether Wnt ligands are important for OSS-mediated *FOXC2* and *GATA2* expression (Cha et al., 2016; Kazenwadel et al., 2015; Sabine et al., 2012), we exposed HLECs to OSS in the presence of recombinant (r) DKK1, which inhibits the interaction between LRP5/6 and Wnt ligands (Mao et al., 2001). The expression of *FOXC2*, *GATA2*, and the positive control *AXIN2* was reduced in OSS-exposed HLECs cultured in the presence of rDKK1 relative to controls (Figure 1B), indicating that Wnt ligands are necessary for OSS-mediated enhancement of *FOXC2* and *GATA2* expression.

To determine whether the Wnt ligands that enhance *FOXC2* and *GATA2* expression are derived from the culture medium or from HLECs, we repeated the OSS experiment in the presence of LGK-974. LGK-974 is a small-molecule inhibitor of the O-acyltransferase Porcupine, which is dedicated to palmitoylating Wnt ligands (Liu et al., 2013). Cells do not secrete Wnt ligands in the absence of palmitoylation. As shown in Figure 1C, OSS is unable to activate the expression of *FOXC2* and *GATA2* in the presence of LGK-974, suggesting that OSS-exposed HLECs secrete canonical Wnt ligands to enhance *FOXC2* and *GATA2* expression in an autocrine manner.

Autocrine Wnt Signaling in LECs Is Dispensable for Lymphatic Vascular Development

To determine whether autocrine Wnt/β-catenin signaling in LECs regulates lymphatic vascular development *in vivo*, we aimed to abolish Wnt ligands from LECs. By RNA sequencing (RNA-seq) of Wnt pathway genes, we determined that at least 10 of the 19 Wnt ligands in mammals are expressed in HLECs (Figure S1A–S1C). It is not feasible to delete all of these Wnt ligands from mouse LECs, so we deleted *Wntless (Wls)*, which encodes a multispan transmembrane protein that regulates the secretion of all Wnt ligands (Carpenter et al., 2010; Logan and Nusse, 2004). Unexpectedly, *Lyve1-Cre;Wls*$^{f/f}$ mice survived to adulthood without any obvious lymphatic vascular defects such as edema (data not shown) and displayed normal LVVs, LVs, and lymphatic vessel size (Figures 1D–1L). These results suggest that LECderived Wnt ligands are dispensable for lymphatic vascular development *in vivo*.

LEC- and Vascular Smooth Muscle Cell-Derived Wnt Ligands Play Complementary Roles during Lymphatic Vascular Development

LVVs develop at the junction of the jugular and subclavian veins in close proximity to the vertebral artery (Geng et al., 2016; Srinivasan and Oliver, 2011). Moreover, lymphatic

vessels generally migrate along the arteries and veins throughout the body (Liu et al., 2016). Therefore, we hypothesized that Wnt signals secreted from blood ECs and/or mural cells influence lymphatic vascular development. To test this, we deleted Wls from all ECs using Tie2-Cre. *Tie2-Cre;Wls*$^{f/f}$ mutants died at E14.5, as reported recently (Franco et al., 2016). However, these embryos did not display any obvious edema, and their LVVs appeared normal, indicating that the blood ECs are not the source of LVV-regulating Wnt ligands (data not shown).

RNA-seq analysis of mural cells obtained from mouse aortae indicated the expression of 10 Wnt ligands (Figure S1D). We deleted Wls in vascular smooth muscle cells using SM22-Cre and determined that SM22-Cre*;Wls*$^{f/f}$ mice die perinatally (data not shown). SM22-Cre;*Wls*$^{f/f}$ possessed LVVs and venous valves (VVs) in the vicinity of LVVs (Figures S2A and S2B, white arrows and yellow arrowheads, respectively). However, E17.5 SM22Cre;*Wls*$^{f/f}$ embryos displayed dysplastic lymphatic vessels that were dilated and reduced in their ability to migrate to the dorsal midline (Figures S2C–S2F, S2M, and S2N). Mutant embryos displayed a mild abnormality in vascular smooth muscle cell recruitment to lymphatic vessels (Figure S2F, arrows). Compared with control littermates, SM22-Cre;*Wls*$^{f/f}$ embryos had fewer LVs in the mesenteric lymphatic vessels (Figures S2G, S2H, and S2O). Interestingly, VEGFR3 expression was not upregulated in the remaining PROX1^{high};FOXC2^{high} mesenteric LV clusters of SM22-Cre;*Wls*$^{f/f}$ embryos, indicating a defect in LV maturation (Figures S2G–S2L, yellow arrows). Thus, Wnt ligands from vascular smooth muscle cells regulate lymphatic vascular development. However, because the lymphatic vascular defects are not fully penetrant in the SM22-Cre;*Wls*$^{f/f}$ embryos, other sources of Wnt ligands likely exist.

We hypothesized that vascular smooth muscle cell-derived Wnt ligands complement LEC-derived Wnt ligands during lymphatic vascular development. To test this hypothesis, we first examined whether a Wnt agonist could enhance OSS-mediated Wnt/β-catenin signaling in HLECs. We cultured HLECs in the presence of OSS, the Wnt agonist 6-Bromoindirubin-3'oxime (BIO) (Sato et al., 2004), or both and evaluated FOXC2 expression. We observed stronger upregulation of FOXC2 in HLECs exposed to both OSS and BIO than with either treatment alone (Figure 2A). Thus, a Wnt agonist could enhance OSS-mediated Wnt/β-catenin signaling to upregulate FOXC2 expression.

To examine whether vascular smooth muscle cell-derived Wnt ligands complement LEC-derived Wnt ligands *in vivo*, we generated SM22-Cre*;Lyve1-Cre;Wls*$^{f/f}$ embryos in which *Wls* is deleted in both vascular smooth muscle cells and LECs. First we confirmed that SM22-Cre;*Lyve1-Cre;R26*$^{+/tdTomato}$ embryos display efficient Cre-dependent labeling of both cell types (Figure S3). We found that E14.5 SM22-Cre;*Lyve1-Cre;Wls*$^{f/f}$ embryos have gross edema and lack LVVs (Figures 2B and 2C, arrows; data not shown). LVVs and VVs were absent in E16.5 SM22-Cre;*Lyve1-Cre;Wls*$^{f/f}$ embryos (data not shown). Mesenteric LVs were absent in E18.5 SM22-Cre;*Lyve1-Cre;Wls*$^{f/f}$ embryos (Figures 2D–2G). Furthermore, whole-mount immunohistochemistry (IHC) showed that the mutant lymphatic vessels were more dilated, had fewer branch points, had migration defects, and were devoid of filopodia (Figures 2H–2M). Thus, LECs complement vascular smooth muscle cells in providing Wnt ligands that are essential for lymphatic vascular development.

We did not observe any obvious changes in capillary density in SM22-Cre; *Wls*$^{f/f}$ or SM22-Cre; *Lyve1-Cre;Wls*$^{f/f}$ embryos (data not shown). We also did not observe any obvious changes in vascular smooth muscle cell coverage on major arteries or veins in these mutants. The diameters and branch points of capillaries and major vessels also appeared to be grossly normal. Interestingly, we observed that the major arteries and veins were avoiding a small region along the midline of Sm22-Cre; *Wls*$^{f/f}$ embryos (Figure S4). Importantly, this defect is not obviously aggravated in Sm22-Cre; *Lyve1-Cre;Wls*$^{f/f}$ embryos. This observation suggests that the more severe lymphatic defects that are seen in Sm22-Cre; *Lyve1-Cre;Wls*$^{f/f}$ embryos (compared with Sm22Cre; *Wls*$^{f/f}$ embryos) are not likely due to blood vascular defects.

Wnt/β-Catenin Signaling via LRP5/6 Is Necessary for Lymphatic Vascular Development

Deletion of Wls abolished both canonical (Wnt/β-catenin) and non-canonical (planar cell polarity and calcium) Wnt signaling pathways. To specifically examine Wnt/β-catenin signaling during lymphatic vasculature development, we deleted LRP5 and LRP6 in LECs using *Lyve1-Cre. Lrp* double-heterozygous (*Lyve1-Cre;Lrp5*$^{+/f}$*;Lrp6*$^{+/f}$) or single-homozygous (*Lyve1Cre;Lrp5*$^{f/f}$ *or Lyve1-Cre;Lrp6*$^{f/f}$) mice survived to adulthood, as did mice lacking up to 3 alleles of *Lrp*. However, *Lyve1-Cre;Lrp5*$^{f/f}$*;Lrp6*$^{f/f}$ pups did not survive past birth (data not shown). We observed mild edema in a subset of E14.5 *Lyve1Cre;Lrp5*$^{f/f}$*;Lrp6*$^{f/f}$ embryos (Figure 3B). Unlike E16.5 control embryos, E16.5 *Lyve1-Cre;Lrp5*$^{f/f}$*;Lrp6*$^{f/f}$ embryos lacked LVVs and VVs (Figures 3D and 3E). Surprisingly, *Lyve1-Cre;Lrp5*$^{f/f}$*;Lrp6*$^{f/f}$ E18.5 embryos had normal-looking lymphatic vessels in the dorsal skin and mesentery (Figures 3H, 3K, and 3N) and displayed LVs within the lymphatic vessels (Figures 3H, 3K, and 3N, arrows, and 3P). We considered that the normal lymphatic vessels and LVs in *Lyve1-Cre;Lrp5*$^{f/f}$*;Lrp6*$^{f/f}$ embryos arise from residual Wnt/β-catenin signaling; for instance, because of incomplete *Lyve1-Cre*-mediated deletion of *Lrp5*$^{f/f}$*;Lrp6*$^{f/f}$ or insufficient depletion of LRP proteins after genetic deletion. To reduce any residual Wnt/β-catenin signaling downstream of LRP5/6, we deleted one allele of Ctnnb1 in the LRP5/6-null background. No obvious defects were observed in the major blood vessels or blood capillaries in the dorsal skin or mesentery of *Lyve1-Cre;Lrp5*$^{f/f}$*;Lrp6*$^{f/f}$ *or Lyve1-Cre;Ctnnb1*$^{+/}$*;LRP5*$^{f/f}$*; LRP6*$^{f/f}$ embryos (data not shown). However, *Lyve1-Cre;Ctnnb1*$^{+/}$*;LRP5*$^{f/f}$*;LRP6*$^{f/f}$ embryos were severely edematous (Figure 3C) and lacked LVVs (Figure 3F). They also lacked LVs in the dorsal skin and in the mesenteric lymphatic vessels (Figures 3I, 3L, 3O, and 3P). Their dorsal skin displayed an increase in the diameter of lymphatic vessels and the space without lymphatic vessels (Figures 3Q and 3S). Furthermore, vascular smooth muscle cells were abnormally recruited to the lymphatic vessels of *Lyve1-Cre;Ctnnb1*$^{+/}$*;LRP5*$^{f/f}$*;LRP6*$^{f/f}$ embryos (Figures 3L and 3R). Finally, FOXC2 expression was dramatically downregulated in the LECs of mutant embryos (Figure 3O). PROX1 expression was also modestly reduced in the tip cells of *Lyve1-Cre;Ctnnb1*$^{+/}$*;LRP5*$^{f/f}$*;LRP6*$^{f/f}$ embryos (data not shown). These phenotypes are similar to the *Lyve1-Cre; Ctnnb1*$^{f/f}$ embryos we reported previously (Cha et al., 2016). However, the lymphatic vessels are more dilated in *Lyve1-Cre; Ctnnb1*$^{f/f}$ embryos. The reason for this difference remains to be investigated.

In summary, autocrine and paracrine Wnt ligands from LECs and vascular smooth muscle cells signal via LRP5/6 to regulate lymphatic vascular development.

Prox1 Genetically Interacts with Wnt/β-Catenin Signaling in Lymphatic Vascular Development

To evaluate the role of the master regulator PROX1 in autocrine Wnt/β-catenin signaling in lymphatic vascular development, we deleted *Wls* in LECs using *Prox1*$^{+/Cre}$. *Prox1*$^{+/Cre}$ mice are hap-loinsufficient for *Prox1*, given that one allele of *Prox1* is replaced with the cDNA encoding GFPCre (Srinivasan et al., 2010). Thus, *Prox1*$^{+/Cre}$ mice are devoid of LVVs and have reduced numbers of LECs (Srinivasan and Oliver, 2011). We found that the *Prox1*$^{+/Cre}$;*Wls*$^{f/f}$ embryos were obtained at less than the expected frequency, and none survived past birth (data not shown). The migration of lymphatic vessels toward the dorsal midline is not significantly different between *Prox1*$^{+/Cre}$ and *Prox1*$^{+/Cre}$;*Wls*$^{f/f}$ embryos (data not shown). However, a-smooth muscle cell-actin^{+} (αSMA^{+}) vascular smooth muscle cells abnormally surround the lymphatic vessels in *Prox1*$^{+/Cre}$;*Wls*$^{f/f}$ embryos, likely resulting in lymphatic vascular dysfunction (Figure 4C). These results further support the role of autocrine Wnt/β-catenin signaling in the lymphatic vasculature and suggest that PROX1 might be positively regulating this pathway. However, a contribution of Wnt ligands from other PROX1^{+} cells, such as cardiomyocytes or hepatocytes, cannot be excluded.

To extend our discovery of the crosstalk between PROX1 and Wnt/β-catenin signaling during lymphatic vasculature development, we generated double heterozygote *Prox1*$^{+/Cre}$;*Ctnnb1*$^{+/f}$ embryos and pups (Brault et al., 2001; Srinivasan et al., 2010). These mice would reveal the role of PROX1 in both autocrine and paracrine Wnt/β-catenin signaling. At E18.5, from a total of 180 embryos, we observed normal numbers of *Prox1*$^{+/Cre}$ embryos (23.8%) but fewer than expected numbers of *Prox1*$^{+/Cre}$;*Ctnnb1*$^{+/f}$ littermates (17.2%). Whole-mount IHC using the dorsal skin of *Prox1*$^{+/Cre}$;*Ctnnb1*$^{+/f}$ embryos revealed poorly patterned lymphatic vessels with abundant αSMA^{+} cell coverage (Figures 4D, arrowhead, and 4E). This phenotype is highly reminiscent of *Foxc2*$^{-/-}$ embryos (Petrova et al., 2004), suggesting that FOXC2 might be a target of PROX1 and Wnt synergy. Consistent with this possibility, we observed substantially reduced FOXC2 expression in the LECs of *Prox1*$^{+/Cre}$;*Ctnnb1*$^{+/f}$ embryos (Figure 4H). Additionally, *Foxc2* and *Axin2* expression was reduced in *Prox1*$^{+/Cre}$ LECs compared with wild-type LECs sorted from E17.5 embryos (Figure 4I) and even further reduced in LECs from *Prox1*$^{+/Cre}$;*Ctnnb1*$^{+/f}$ embryos.

Soon after birth, 81.8% of the *Prox1*$^{+/Cre}$ pups developed chylous ascites (leakage of milk in the gut, Figure S5E). Only 18.2% *Prox1*$^{+/Cre}$ pups developed both chylous ascites and chylothorax (milk in the pleural cavity; data not shown), whereas 66.7% of *Prox1*$^{+/Cre}$;*Ctnnb1*$^{+/f}$ pups developed both (Figures S5C and S5F). We first characterized the LVVs of surviving wild-type, *Prox1*$^{+/Cre}$, and *Prox1*$^{+/Cre}$;*Ctnnb1*$^{+/f}$ littermates at post-natal day 5 (P5). Although *Prox1*$^{+/Cre}$ embryos lack LVVs and VVs (Geng et al., 2016; Srinivasan and Oliver, 2011), four of the seven surviving *Prox1*$^{+/Cre}$ pups developed normal LVVs and VVs (Figure S5H, arrows and yellow arrowheads, respectively). Three of the seven animals had one LVV instead two (data not shown). In contrast to *Prox1*$^{+/Cre}$ littermates, three of the four *Prox1*$^{+/Cre}$;*Ctnnb1*$^{+/f}$ pups lacked LVVs and VVs (Figure S5I) and one mutant lacked VVs, although it had a small opening at the LVV-forming region (data not shown).

At P21, from a total of 300 pups, *Prox1*$^{+/Cre}$ and *Prox1*$^{+/Cre}$; *Ctnnb1*$^{+/f}$ pups were observed at 14.3% and 7.3% frequency, respectively (both were expected at 25% frequency). Despite the dramatic defects at the embryonic and early postnatal stages, the surviving *Prox1*$^{+/Cre}$ and *Prox1*$^{+/Cre}$;*Ctnnb1*$^{+/f}$ animals developed LVs in their popliteal lymphatic vessels (Figure S5J; data not shown). To evaluate the function of LVs in a quantitative manner from adult wild-type, *Prox1*$^{+/Cre}$, and *Prox1*$^{+/Cre}$;*Ctnnb1*$^{+/f}$ mice, we utilized a recently described ex vivo, cannulated vessel approach (Lapinski et al., 2017; Figure S5K). Although LVs of *Prox1*$^{+/Cre}$ mice are comparable with control littermates, some LVs of *Prox1*$^{+/Cre}$;*Ctnnb1*$^{+/f}$ mice are leaky (Figure S5L). In addition, most LVs of *Prox1*$^{+/Cre}$;*Ctnnb1*$^{+/f}$ are partially incompetent (requiring higher pressure to close) (Figure S5M). Overall, our data reveal more substantial defects in the LVVs and LVs of *Prox1*$^{+/Cre}$;*Ctnnb1*$^{+/f}$ mice relative to *Prox1*$^{+/Cre}$ mice.

In summary, the phenotypic similarities between *Prox1*$^{+/Cre}$; *Ctnnb1*$^{+/f}$ and *Prox1*$^{+/Cre}$;*Wls*$^{f/f}$ mice suggest that PROX1 genetically interacts with autocrine and paracrine Wnt/β-catenin signaling in LECs to support lymphatic vascular patterning, valve development, and LV functioning.

PROX1 Is Necessary and Sufficient for Wnt/β-Catenin Signaling-Dependent FOXC2 and GATA2 Expression in the Lymphatic Vasculature

To evaluate the role of PROX1 in Wnt/β-catenin signaling, we first compared the Wnt responses of HLECs, which express PROX1, with blood vascular ECs, which do not express PROX1. We found that OSS, recombinant Wnt3a (rWnt3a), and BIO all enhanced the expression of *AXIN2, FOXC2*, and *GATA2* in HLECs (Figures 5A, 5B, and S6A). The pro-lymphangiogenic receptor tyrosine kinase VEGFR3 and the fatty acid oxidation pathway regulator *CPT1a*, which are known targets of PROX1 in LECs, were not affected by OSS, rWnt3a, or BIO (data not shown; Petrova et al., 2002; Srinivasan et al., 2014; Wong et al., 2017). Thus, Wnt/β-catenin signaling activates a specific set of genes in LECs. OSS activates Wnt/β-catenin signaling in PROX1 blood vascular ECs (Li et al., 2014), and we found that OSS, rWnt3a, and BIO enhanced the expression of *AXIN2* in PROX1 human umbilical vein ECs (HUVECs) (Figures 5A, 5B, and S6A). However, OSS, rWnt3a, and BIO did not trigger upregulation of *GATA2* or FOXC2 in HUVECs (Figures 5A, 5B, and S6A). These data suggest that upregulation of *GATA2* and *FOXC2* via Wnt/β-catenin signaling requires an additional factor that is present in HLECs but not in HUVECs.

To determine whether PROX1 is the factor that cooperates with Wnt/β-catenin signaling to activate the expression of *FOXC2* and *GATA2*, we ectopically expressed PROX1 in HUVECs and exposed the cells to either OSS (Figure 5C) or BIO (Figure 5D). We found that OSS exposure enhanced FOXC2 expression in PROX1^{+} HUVECs compared with PROX1^{-} HUVECs (Figure 5C) and that BIO treatment similarly enhanced *FOXC2* and *GATA2* expression (Figure 5D). To determine whether Wnt/β-catenin signaling is required for PROX1-mediated regulation of FOXC2, we utilized the Wnt antagonist iCRT3, which inhibits the interaction between β-catenin and TCF/LEF transcription factors (Gonsalves et al., 2011). We found that FOXC2 expression is inhibited by iCRT3 in both static and OSS-

treated PROX1$^+$ HUVECs (Figure 5C). Thus, PROX1 promotes the induction of *FOXC2* and *GATA2* in HUVECs via Wnt/β-catenin signaling.

To evaluate whether PROX1 is required for Wnt/β-catenin signaling-mediated induction of *FOXC2* and *GATA2* in HLECs, we used RNAi to generate PROX1 knockdown HLECs. Specifically, we infected HLECs with lentiviruses expressing distinct short hairpin RNAs (shRNAs) targeting PROX1 (sh-PROX1#1 and sh-PROX1#2) and confirmed reduced expression of PROX1 and its target genes *VEGFR3* and *CPT1a* (Figure S6B). In contrast to control cells, OSS, rWnt3a and BIO did not induce *FOXC2* or *GATA2* in PROX1 knockdown cells (Figures 5E, 5F, and S6C).

Together, our data suggest that Wnt/β-catenin signaling requires PROX1 to enhance *FOXC2* and *GATA2* expression in HLECs.

PROX1 Physically Interacts with β-Catenin and TCF7L1

We noticed that expression of the constitutive Wnt/β-catenin target genes *AXIN2, cMYC* and *cJUN* was also reduced in PROX1 knockdown HLECs relative to controls (Figure 6A). To extend these findings, we performed TOPFlash-luciferase reporter analyses in 293T cells (Korinek et al., 1997). Activation of Wnt/β-catenin signaling leads to β-catenin nuclear translocation, where it interacts with TCF/LEF transcription factors to activate target genes containing TCF sites. The TOPFlash-luciferase reporter contains wild-type TCF upstream of luciferase. We found that PROX1 was sufficient to activate the TOPFlash reporter and that co-expression of PROX1 with β-catenin synergistically activated the TOPFlash reporter (Figure 6B). In contrast, a mutant FOPFlash reporter, which contains mutated TCF/LEF binding sites, did not respond to PROX1 (Figure 6B). Further, co-expression of AXIN, a key component of the β-catenin destructive complex (Logan and Nusse, 2004), or of a dominant-negative form of TCF7L2 (DN-TCF7L2) that associates with the DNA but not with β-catenin because of N-terminal deletion (Korinek et al., 1997), both antagonized PROX1-dependent TOPFlash reporter activity (Figures 6C and 6D). These results indicate that PROX1 might be regulating the core components of Wnt/β-catenin signaling.

PROX1 has been shown to upregulate β-catenin expression in hepatocellular carcinoma cell lines (Liu et al., 2015). However, we did not observe significant changes in β-catenin expression in PROX1 knockdown HLECs or in PROX1$^+$ HUVECs relative to controls (data not shown). Several transcription factors and cofactors interact with β-catenin to control cell fate during development (Fiedler et al., 2015; Olson et al., 2006; Sustmann et al., 2008). To investigate whether PROX1 interacts with β-catenin, we performed co-immunoprecipitation (coIP) analyses. We found that FLAG-tagged PROX1 interacts with Myc-tagged β-catenin in 293T cells (Figure 6E). Further, endogenous PROX1 and β-catenin interact by coIP in HLECs (Figure 6F), and treatment of HLECs with BIO enhanced the PROX1/β-catenin interaction in a time-dependent manner (Figure 6G).

We previously showed that β-catenin directly associates with the regulatory elements of *FOXC2* in BIO-treated HLECs (Cha et al., 2016). To investigate whether PROX1 associates with *FOXC2* regulatory elements, we performed chromatin immunoprecipitation (ChIP). Indeed, we found that PROX1 associates with the β-catenin binding site in *FOXC2* in BIO-

treated HLECs (Figure 6H). This result suggests that Wnt/β-catenin signaling triggers the recruitment of the PROX1/β-catenin complex to the regulatory elements of *FOXC2*.

Nuclear β-catenin associates with TCF/LEF transcription factors to activate its target genes (Schuijers et al., 2014). There are four TCF/LEF factors in mammals: TCF7, TCF7L1, TCF7L2, and LEF1 (Logan and Nusse, 2004). Our RNA-seq data revealed that TCF7L1 and TCF7L2 are expressed in HLECs (Figure S1A). By qRT-PCR and by IHC, we verified that TCF7L1 is expressed in mouse embryonic LECs (data not shown). A mutant of TCF7L1, DN-TCF7L1, associates with DNA but not with β-catenin and, thus, disrupts Wnt/β-catenin signaling. Most $TCF7L1^{\Delta N/\Delta N}$ embryos develop a severe edematous phenotype (Wu et al., 2012). We did not observe any obvious blood vascular defects in the dorsal skin or mesentery of $TCF7L1^{\Delta N/\Delta N}$ embryos (data not shown). However, we found that $TCF7L1^{\Delta N/\Delta N}$embryos lacked LVVs and VVs (Figures 7A and 7B, arrows and yellow arrowheads, respectively). The dermal lymphatic vessels of $TCF7L1^{\Delta N/\Delta N}$embryos were dilated, and their migration was defective (Figures 7C–7F and S7A–S7D). Further, αSMA^{+} mural cells were abnormally recruited to the lymphatic vessels of the skin in $TCF7L1^{\Delta N/\Delta N}$ embryos (Figures 7H, yellow arrowheads, and 7I), and LVs did not form in dorsal skin and mesenteric lymphatic vessels (Figures 7J–7L and S7E–S7H). Thus, $TCF7L1^{\Delta N/\Delta N}$ embryos phenocopy embryos lacking β-catenin or it target FOXC2, suggesting that this TCF contributes to most of the Wnt/β-catenin signaling in the developing lymphatic vasculature. However, we cannot exclude a noncell-autonomous role for TCF7L1 during lymphatic vascular development.

Next we determined whether the TCF7L1-β-catenin interaction is necessary for OSS-induced Wnt/β-catenin signaling in HLECs. Indeed, we found that ectopic expression of DNTCF7L1 inhibited OSS-mediated induction of *AXIN2, FOXC2,* and *GATA2* in HLECs, suggesting that the TCF7L1-β-catenin interaction underlies the OSS response in HLECs (Figure 7M).

TCF/LEF transcription factors directly associate with DNA and activate genes in a β-catenin-dependent manner. Given our observation that β-catenin physically interacts with PROX1, we asked whether PROX1 also interacts with TCF7L1. We performed a coIP assay with 293T cells expressing PROX1 and/or FLAG-tagged TCF7L1 and observed an interaction between PROX1 and FLAG-TCF7L1 (Figure 7N). Interestingly, FLAGTCF7L1 enhanced the interaction between PROX1 and β-catenin. To determine whether PROX1 interacts with TCF7L1 directly or indirectly through β-catenin, we performed the coIP assay using epitope-tagged FLAG-ΔN-TCF7L1. We found that PROX1 did not interact with ΔN-TCF7L1, suggesting that the PROX1TCF7L1 interaction requires β-catenin (Figure 7N). These data suggest that PROX1 forms a transcriptional complex with β-catenin and TCF7L1.

In summary, these results support a model in which PROX1 is required for Wnt/β-catenin signaling during development of the lymphatic vasculature. PROX1 interacts with β-catenin and TCF7L1 in a Wnt/β-catenin signaling-dependent manner, and both β-catenin and PROX1 target FOXC2 in the lymphatic vasculature.

DISCUSSION

Here, we show that development of the lymphatic vasculature requires Wnt ligands derived from LECs and vascular smooth muscle cells. Our work also shows that PROX1 cooperates with Wnt/β-catenin to activate *GATA2* and *FOXC2* and other Wnt/β-catenin target genes in LECs. This mechanism is at least in part mediated by the interaction of the PROX1/β-catenin/ TCF7L1 complex on the regulatory elements of *FOXC2*. Our results are summarized in Figure S8.

Lymphatic Vasculature-Specific Roles of Wnt Signaling

In the intestinal epithelium, Paneth cells are considered the source of Wnt ligands that regulate the differentiation and proliferation of epithelial stem cells in *ex vivo* organoids (Sato et al., 2011). However, abolishing Wnt secretion from Paneth cells does not significantly affect intestinal epithelial homeostasis *in vivo* (Kabiri et al., 2014). Stromal cells that are located near the intestinal crypts produce Wnt ligands and compensate for the loss of Paneth cell-derived Wnt ligands (Kabiri et al., 2014). In a similar manner, although autocrine Wnt/β-catenin signaling is sufficient for activating the expression of FOXC2 and GATA2 *in vitro*, Wnt ligands from vascular smooth muscle cells play a complementary role *in vivo.*

Wnt/β-catenin signaling controls context-dependent gene regulation. For example, Wnt3a induces the expression of 355 genes in NIH 3T3 cells but only 129 genes in PC12 cells. Furthermore, only two of the Wnt-induced genes are common between the two cell lines (Railo et al., 2009). Likewise, although β-catenin activates Cyclin-D1 expression in neural progenitor cells, it activates the expression of neurogenin-2 but not Cyclin-D1 in neurons (Qu et al., 2013). Similar to these findings, we have now identified *FOXC2* and *GATA2* as target genes of Wnt/β-catenin signaling in LECs but not in blood ECs. The transcription factor PROX1 is necessary for this tissue-specific response.

We have shown that TCF7L1 interacts with PROX1 and β-catenin. Furthermore, we have shown that the dominant-negative form of TCF7L1 inhibits lymphatic vascular development. The dominant-negative form of TCF7L1 likely inhibits the transcriptional activity of all TCF/LEF transcription factors. In addition to TCF7L1, TCF7L2 is expressed in HLECs (Figure S1A). Whether TCF7L1 and TCF7L2 can compensate for each other in LECs remains to be elucidated.

Shear Stress and Lymphatic Vascular Development

Lymph flows in a reciprocating manner within the lymphatic vessels, with LVs ensuring that net lymph flow is forward (Sweet et al., 2015). OSS generated by lymph flow was proposed to regulate the maturation of lymphatic vessels and the development of LVs (Sabine et al., 2012; Sweet et al., 2015). Targets of OSS in LECs include the lymphedema-associated transcription factors *FOXC2* and *GATA2*, the gap junction protein Connexin 37 (*CX37*), integrin-a9 (*ITGA9*), and *ephrin-B2*, all of which are necessary for lymphatic vessel morphogenesis and/or LV formation. OSS activates the transcriptional activity of HDAC3 to enhance GATA2 expression (Janardhan et al., 2017). Nevertheless, technical difficulties have

limited our insight into the role of OSS during lymphatic vascular development, and some differences exist between the “OSS model” and *in vivo* observations (Geng et al., 2017). Hence, it is important to evaluate the significance of OSS during lymphatic vascular development by using a combination of in vitro assays and genetic tools. Our *in vitro* assays show that OSS promotes Wnt/β-catenin signaling through Wnt ligands. OSS does not seem to increase the expression of Wnt ligands (data not shown) but might promote their secretion. Our in vivo data suggest that OSS-mediated, autocrine Wnt/β-catenin signaling in LECs is complemented by paracrine signaling via vascular smooth muscle cell derived Wnt ligands. *In vivo*, LECs are always exposed to some form of OSS (Sweet et al., 2015). It is possible that OSS-exposed LECs represent the “natural ground state” of LECs upon which extrinsic signals act and promote further differentiation. In support of this possibility, Wnt agonists promote a much stronger expression of FOXC2 compared with OSS (Figure 2A).

PROX1, the Master Regulator of Lymphatic Vascular Development

PROX1 is the most upstream regulator of lymphatic vascular development. *Prox1*$^{-/-}$ mice lack LECs, and deleting even one allele of Prox1 is sufficient to cause lymphatic vessel hypoplasia and prevent the formation of VVs and LVVs (Geng et al., 2016; Harvey et al., 2005; Johnson et al., 2008; Srinivasan and Oliver, 2011). Lymphatic valve development is also compromised in Prox1$^{+/-}$ mice (Johnson et al., 2008). Here, we have shown that PROX1 associates with the β-catenin complex to enhance Wnt/β-catenin signaling and to regulate the expression of *GATA2* and *FOXC2*. Interestingly, Wnt/β-catenin signaling enhances PROX1 expression in LECs (Cha et al., 2016). Therefore, there is a feedback loop operating between PROX1 and Wnt/β-catenin signaling, which could explain the higher levels of PROX1 expression in valvular ECs.

Feedback loops are routinely used during organogenesis to establish lineage identity (Ptashne, 2007). We and others previously reported a feedback regulation between PROX1 and its downstream target VEGFR3 during the differentiation of LECs from venous ECs (Koltowska et al., 2015; Srinivasan et al., 2014). VEGFR3 signaling is critical for the growth and patterning of lymphatic vessels. However, whether VEGFR3 is important for valve formation is currently unclear. VEGFR3 is strongly expressed in LVs but only modestly expressed in LVV-ECs and VVs (Bazigou et al., 2009; Geng et al., 2016). VEGFR3 expression is not properly upregulated in Sm22Cre;*Wls*$^{f/f}$ embryos. The relationship between the Wnt/β-catenin and VEGFR3 signaling pathways remains to be elucidated. Nevertheless, it is interesting that PROX1 is at the center of two critical signaling pathways. We speculate that PROX1 functions as a hub where various input signals are integrated to determine the proper output. PROX1 might be regulating this process at least in part by its protein interaction network. PROX1 interacts with β-catenin, ETS transcription factors, the orphan nuclear hormone receptor COUP-TFII, and the mechanosensory transcription factor KLF2 in LECs (Choi et al., 2017; Srinivasan et al., 2010; Yoshimatsu et al., 2011). It is conceivable that subtle changes in the composition of the PROX1 complex, which are initiated by the input signals, lead to distinct outcomes.

In summary, our work further strengthens the prevailing idea that PROX1 is a master regulator of lymphatic vascular development (Bixel and Adams, 2008; Hong and Detmar,

2003). We propose that PROX1 controls the development of some tissues by acting as a tissue-specific co-regulator of Wnt/β-catenin signaling. Further genomic, proteomic, and systems biology approaches are needed to characterize the relationship between PROX1 and Wnt/β-catenin signaling.

STAR*METHODS

KEY RESOURCES TABLE

REAGENT or RESOURCE	SOURCE	IDENTIFIER
Antibodies		
Rabbit anti-PROX1 antibody	AngioBio	Cat# 11–002; RRID: AB_10013720
Goat anti-human PROX1 antibody	R&D	Cat# AF2727; RRID: AB_2170716
Sheep anti-mouse FOXC2 antibody	R&D	Cat# AF6989; RRID: AB_10973139
Goat anti-mouse VEGFR3 antibody	R&D	Cat# AF743; RRID: AB_355563
Rat anti-mouse CD31 antibody	BD PharMingen	Cat# 553370; RRID: AB_394816
Rat anti-mouse Endomucin antibody	Thermo Fisher Scientific	Cat# 14–5851-81; RRID: AB_891529
Mouse Cy3-conjugated anti-aSMA antibody	Sigma-Aldrich	Cat# C6198; RRID: AB_476856
Mouse anti-β-Actin antibody	Sigma-Aldrich	Cat# A5441; RRID: AB_476744
Mouse anti-mouse β-Catenin antibody	BD Biosciences	Cat# 610154; RRID: AB_397555
Mouse anti-human LRP6 antibody	Santa Cruz Biotechnology	Cat# sc-25317; RRID: AB_627894
Rabbit anti-human phospho-LRP6 antibody	Cell Signaling Technology	Cat# 2568; RRID: AB_2139327
Mouse anti-Myc tag antibody	Applied Biological Materials Inc	Cat# G019; RRID: N/A
Mouse anti-Flag tag antibody	Sigma-Aldrich	Cat# F3165; RRID: AB_259529
Goat anti-mouse VEGFR3 biotinylated antibody	R&D	Cat# BAF743; RRID: AB_2104991
Donkey Cy3-conjugated anti-rabbit secondary antibody	Jackson ImmunoResearch Labs	Cat# 711–165-152; RRID: AB_2307443
Donkey Cy3-conjugated anti-sheep secondary antibody	Jackson ImmunoResearch Labs	Cat# 713–165-147; RRID: AB_2315778
Donkey Cy5-conjugated anti-rat secondary antibody	Jackson ImmunoResearch Labs	Cat# 712–175-150; RRID: AB_2340671
Donkey Alexa Fluor 488-conjugated anti-goat secondary antibody	Jackson ImmunoResearch Labs	Cat# 705–545-147; RRID: AB_2336933
Donkey Alexa Fluor 488-conjugated anti-rat secondary antibody	Molecular Probes	Cat# A-21208; RRID: AB_141709
Donkey IgG-HRP anti-sheep secondary antibody	Santa Cruz Biotechnology	Cat# sc-2473; RRID: AB_641190
Donkey IgG-HRP anti-goat secondary antibody	Santa Cruz Biotechnology	Cat# sc-2020, RRID: AB_631728

Goat IgG-HRP anti-mouse secondary antibody	Santa Cruz Biotechnology	Cat# sc-2005, RRID: AB_631736
Goat IgG-HRP anti-rabbit secondary antibody	Santa Cruz Biotechnology	Cat# sc-2030, RRID: AB_631747
Bacterial and Virus Strains		
DH5α Competent Cells	Thermo Fisher Scientific	Cat# 18265017
pLV-mCherry	This paper	N/A
pLV-mCherry-PROX1	This paper	N/A
pLV-EGFP-Flag-TCF7L1	This paper	N/A
pLV-EGFP-Flag-ΔN-TCF7L1	This paper	N/A
pLV[shRNA]-EGFP-control	This paper	N/A
pLV[shRNA]-mCherry-PROX1-shRNA#1	This paper	N/A
pLV[shRNA]-EGFP-PROX1-shRNA#2	This paper	N/A
Chemicals, Peptides, and Recombinant Proteins		
Recombinant Human Wnt-3a Protein	R&D	Cat# 5036-WN
Recombinant Human Dkk-1 Protein	R&D	Cat# 5439-DK
BIO	Sigma-Aldrich	Cat# B1686
iCRT3	Sigma-Aldrich	Cat# SML0211
LGK-974	Selleckchem	Cat# S7143
Human Fibronectin	Corning	Cat# 354008
Dispase II	GIBCO	Cat# 17105041
Collagenase	GIBCO	Cat# 17100017
Osmium Tetroxide	Electron Microscopy Sciences	Cat# 19190
Hexamethyldisilazane	Acros	Cat# 120585000
Critical Commercial kits and assays		
DMEM	Corning	Cat# 10–013-CV
Penicillin-Streptomycin	GIBCO	Cat# 15–140-148
FBS	VWR	Cat# 3100–500
X-tremeGene 9 DNA Transfection Reagent	Roche	Cat# 06365787001
Trizol	Thermo Fisher Scientific	Cat# 15596026
PowerUp SYBR Green Master Mix	Applied Biosystems	Cat# A25742
iScript Advanced cDNA Synthesis Kit	Bio-Rad	Cat# 172–5038
Pierce BCA Protein Assay Kit	Thermo Fisher Scientific	Cat# 23227
Dual-Luciferase Reporter 1000 Assay System	Promega	Cat# E1980
SuperSignal West Femto Maximum Sensitivity Substrate Kit	Thermo Fisher Scientific	Cat# 34095
EZ ChIP Kit	Millipore Sigma	Cat# 17–371
EGM-2 EC Growth Medium-2 Bullet Kit	Lonza	Cat# CC-4176
MACS Cell Separation Columns	Miltenyi Biotec	Cat# 130–042-201
Anti-Biotin Microbeads	Miltenyi Biotec	Cat# 130–090-485
Experimental Models: Cell Lines		

HEK293T	ATCC	Cat# ACS-4500
HUVEC	Thermo Fisher Scientific	Cat# C-015–10C
Human neonatal dermal lymphatic endothelial cells (HLECs): HMVEC-dLyNeo-Der	Lonza	Cat# CC-2812
Experimental Models: Organisms/Strains		
Mouse: *Prox1*$^{+/Cre}$	(Srinivasan et al., 2010)	N/A
Mouse: *Tcf7l1*$^{+/\Delta N}$	(Wu et al., 2012)	N/A
B6.129-Ctnnb1^{tm2Kem}/KnwJ (Ctnnb1$^{+/f}$)	(Brault et al., 2001)	Cat# JAX:004152; RRID: IMSR_JAX: 004152
B6;129-Lrp5$^{tm1.1Vari}$*/J (Lrp5*$^{+/f}$*)*	(Joeng et al., 2011)	Cat# JAX:026269; RRID: IMSR_JAX: 026269
B6;129S-Lrp6$^{tm1.1Vari}$*/J (Lrp6*$^{+/f}$*)*	(Joeng et al., 2011)	Cat# JAX:026267; RRID: IMSR_JAX: 026267
129S-W/s$^{tm1.1Lan}$*/J (W/s*$^{+/f}$)	(Carpenter et al., 2010)	Cat# JAX:012888; RRID: IMSR_JAX: 012888
B6;129P2-Lyve1$^{tm1.1(EGFP/cre)Cys}$*/J (Lyve1-Cre)*	(Pham et al., 2010)	Cat# JAX:012601; RRID: IMSR_JAX: 012601
B6.Cg-Tg(Tek-cre)1Ywa/J (Tie2-Cre)	(Kisanuki et al., 2001)	Cat# JAX:008863; RRID: IMSR_JAX: 008863
B6.Cg-Tg(Tagln-cre)1Her/J (SM22-Cre)	(Holtwick et al., 2002)	Cat# JAX:017491; RRID: IMSR_JAX: 017491
Gt(ROSA)26Sor$^{tm9(CAG-tdTomato)Hze}$ *(R26*$^{+/tdTomato}$*)*	(Madisen et al., 2010)	Cat# JAX:007909; RRID: IMSR_JAX: 007909
Oligonucleotides		
Please see Table S1	N/A	N/A
Recombinant DNA		
pCS2-Myc-β-catenin	This paper	N/A
pCS2-Myc-tagged Axin1	This paper	N/A
pSuper-TOPFlash	Addgene	Cat# 12456
pSuper-FOPFlash	Addgene	Cat# 12457
pLV-mCherry	This paper	N/A
pLV-mCherry-PROX1	This paper	N/A
pLV-EGFP-Flag-TCF7L1	This paper	N/A
pLV-EGFP-Flag-ΔN-TCF7L1	This paper	N/A
pLV[shRNA]-EGFP-control	This paper	N/A
pLV[shRNA]-mCherry-PROX1-shRNA#1	This paper	N/A
pLV[shRNA]-EGFP-PROX1-shRNA#2	This paper	N/A
Software and Algorithms		

Adobe Photoshop	Adobe system	https://www.adobe.com/products/photoshop.html
ImageJ	N/A	https://imagej.nih.gov/ij/
GraphPad Prism 7	GraphPad Software Inc	https://www.graphpad.com/scientific-software/prism/
Excel	Microsoft	https://products.office.com/en-US/compare-all-microsof

CONTACT FOR REAGENT AND RESOURCE SHARING

Request for reagents must be directed to the Lead Contact, R. Sathish Srinivasan (Sathish-srinivasan@omrf.org). The requests will be fulfilled with simple Material Transfer Agreement (MTA).

EXPERIMENTAL MODEL AND SUBJECT DETAILS

Mice—We used mice in these studies. Mice were of mixed background (C57BL6 and NMRI). Both male and female mice were used for the experiments. Female mice of reproductive age (> 6 weeks) were used for generating embryos. All mice were housed and handled according to the institutional IACUC protocols.

Cell lines—De-identified primary human lymphatic endothelial cells were purchased from Lonza and de-identified primary human umblical vein ECs were purchased from Thermo Fisher Scientific. HEK293T human embryonic kidney cells were from ATCC. All human cells were treated as potential biohazards and handled according to institutional biosafety regulations.

METHOD DETAILS

Cell culture and oscillatory shear stress (OSS)—HEK293T human embryonic kidney cells were grown in Dulbecco's modified Eagle's medium (Invitrogen, Carlsbad, CA, USA) supplemented with 10% fetal bovine serum (Sigma-Aldrich, St. Louis, MO, USA) and 100 U/ml penicillin-streptomycin (Sigma-Aldrich, St. Louis, MO, USA). We obtained primary human lymphatic endothelial cells (HLECs) from Lonza and primary human umbilical vein ECs (HUVECs) from Thermo Fisher Scientific. HLECs and HUVECs were seeded on fibronectin-coated plates and were maintained in EGM-2 EC Growth Medium-2 Bullet Kit (Lonza). All experiments were conducted using passage 6–7 cells.

Recombinant Wnt3a and recombinant DKK1 were purchased from R&D systems. The proteins were solubilized in sterile PBS and added to the culture media at a concentration of 200 ng/ml and 100 ng/ml respectively. Wnt agonist BIO and antagonist iCRT3 were purchased from Sigma-Aldrich and used at a concentration of 0.5 μM and 20 μM respectively. Porcupine inhibitor LGK-974 was purchased from Selleckchem and used at a concentration of 2 μM.

OSS experiments were performed according to our previous protocol (Cha et al., 2016). Briefly, HLECs and HUVECs were cultured to 95% confluency in six-well plates and exposed to OSS using a test tube rocker (Thermolyne Speci-Mix aliquot mixer model M71015, Barnstead International) with a preset frequency (18 rpm). 6 mL of medium was used to cover six-well plates. Based on calculation that was described previously the cells

are exposed to an OSS shear stress of 0.3 dynes/cm^2. The entire experiment was performed inside a sterile humidified incubator with 5% CO_2 for 48 h.

Cell sorting—Mouse LECs were isolated from the dorsal skin of E17.5 embryos using a modified version of the protocol described previously (Kazenwadel et al., 2012). Briefly, embryonic skins were dissected in HBSS with 10 μM HEPES and 5% FBS. The isolated skins were individually incubated 10 mL digestion solution (DHF: DMEM/20%FCS/10 μM HEPES) containing Collagenase B (0.05%), Dispase II (2.5U/ml) and DNase I (50mg/ml) at 37C for 30 min. The tissues were sequentially passed through 19, 21 and 24 gauge needles. Skin samples were filtered through a 40 mm cell strainer and rinsed with 2 volumes of ice-cold DHF. Mixed cells from the skins were incubated with goat anti-mouse VEGFR3 biotinylated antibody (R&D Systems, Minneapolis, MN, USA) for 10 min and diluted with 20 volumes MACS Buffer (PBS, 2 mM EDTA, 5% FBS). Cell suspension was incubated with 100 mL of anti-biotin micro beads (Miltenyi Biotec, Bergisch Gladbach, Germany) for 10 min. Subsequently cells were sorted by MACS MS columns according to manufacturer's instructions (Miltenyi Biotec, Bergisch Gladbach, Germany).

Chromatin Immunoprecipitation—ChIP assays were performed using EZ-ChIP kit (MilliporeSigma, Burlington, MA, USA) according to the manufacturer's instructions. Briefly, 1.0 X 10^7 HLECs (Lonza) at 90% confluency were treated with DMSO or Bio (0.5 μM) for 3 hours. Subsequently, HLECs were fixed in 1% formaldehyde for 10 min at room temperature and glycine at a final concentration of 0.125 M was added for 5 min. Cells were washed with 20 mL of cold PBS twice (ten minutes each) and harvested. Cells were lysed and sonicated as described previously described (Cha et al., 2016). Chromatin immunoprecipitation was performed using 3.0 mg of rabbit anti-PROX1 (AngioBio, San Diego, CA, USA) or 1.0 mg of rabbit IgG antibody (Santa Cruz Biotechnology, Dallas, TX, USA). QRT-PCR was performed as described our previous report (Cha et al., 2016) using primers flanking the predicted TCF/LEF sites or control sites. Primer sequences are provided in the Table S1.

IHC—IHC on sections and whole mount IHC were done according to our previously published protocols (Cha et al., 2016; Geng et al., 2016). Briefly, for cryosections we collected embryos and fixed them in 4% PFA overnight at 4°C. The embryos were washed three times (10 minutes each) in cold PBS. Embryos were transferred to 15% sucrose and incubated overnight at 4°C. Subsequently, the samples were transferred to 30% sucrose and incubated at 4°C until they are completely immersed in the solution. Embryos were then cryo embedded in OCT solution (Sakura, Tokyo, Japan). 12 μm cryosections were prepared using a cryotome and IHC was performed using the indicated antibodies.

Embryos were analyzed at E13.5, E14.5, E15.5, E16.5 and E18.5 and data from one representative stage is presented. At least three controls and three mutants are analyzed per stage. Embryos are sectioned in dorsal to ventral orientation along the entire width of the jugular vein. Several consecutive 12 mm sections are analyzed to determine whether LVVs and VVs are present or absent or reduced in size.

Whole-mount IHC using embryonic skins or guts was performed according to our previously published protocol (Cha et al., 2016). Embryos were harvested and fixed in 1% PFA overnight at 4°C. Then, skins and guts were isolated and additionally fixed in 1% PFA for 1 hour. Subsequently, samples were immunostained using the iDISCO protocol with small modifications (Renier et al., 2014). Specifically, PFA fixed tissues were not pretreated with methanol and they were not cleared after immunostaining. Samples were visualized and analyzed as described previously (Cha et al., 2016).

Immunoprecipitation and western blotting—Cells were lysed in lysis buffer (20mM Tris–HCl (pH 7.5), 150mM NaCl, 1.0% Triton X-100, 20mM NaF, 2mM EDTA, 2mM Na-orthovanadate, 1mM phenylmethylsulfonyl fluoride (PMSF), 5 mg/ml leupeptin A). Lysates were cleared by centrifugation for 15 min at 15,000 g and the supernatant was collected and used for immunoprecipitation and immunoblotting. Protein concentration was measured using BCA protein assay kit (Thermo Fisher Scientific, MA, USA). Immunoprecipitations were performed as previously described (Cha et al., 2011). Briefly, 600 – 1000 mg of cell lysate was incubated overnight with the appropriate antibodies overnight at 4C. The immunoprecipitates were resolved by SDS–PAGE and analyzed by immunoblotting using standard protocols. Mouse anti-Myc (Applied Biological Materials Inc, Richmond, BC, Canada), mouse anti-Flag (Sigma-Aldrich, St. Louis, MO, USA) and rabbit anti-PROX1 (AngioBio, San Diego, CA, USA) antibodies were used for the coimmunoprecipitation assays.

Lentiviral transduction—pLV lentiviral plasmids were used for overexpression or knock-down studies. Human PROX1 (NM_002763.4), TCF7L1 (NP_112573.1) and dominant negative (ΔN)-TCF7L1 (deletion of the first 74 first amino acids of TCF3) were cloned into pLV to generate pLV-mCherry-PROX1, pLV-EGFP-Flag- TCF7L1 and pLV-EGFP-Flag-ΔN-TCF7L1 respectively. To knock down human PROX1 gene in HLECs PROX1-shRNA#1 (target sequence TTTCCAGGAGCAACCATAATT) and PROX1-shRNA#2 (target sequence AGTACATCAGGAGGATATATG) were cloned into a pLV plasmid to generate pLV[shRNA]-mCherry-PROX1-shRNA#1 and pLV [shRNA]-EGFP-PROX1-shRNA#2 respectively. Cyagen Biosciences (Santa Clara, CA, USA) generated the lentiviral particles using LentiPAC 293 cells. Cells were infected according to the manufacturer's instructions. Cyagen provided the pLV-mCherry and pLV [shRNA]-EGFP-control viruses.

Luciferase reporter assays—Luciferase assays protocol was as described previously (Cha et al., 2011). To measure luciferase activity HEK293T cells were cotransfected with TOPFlash or FOPFlash luciferase reporter plasmids together with PROX1, β-catenin, AXIN or ΔN-TCF7L2 expression plasmids. X-tremeGene 9 DNA Transfection Reagent (Roche, Mannheim, Germany) was used according to manufacturer's instruction for transfection. pTK-Renilla (Promega, Madison, WI, USA) as an internal control to determine transfection efficiency. Luciferase activity was measured 36 hr later using Dual luciferase reporter assay kit (Promega, Madison, WI, USA) according to the manufacturer's instructions.

RNA isolation and quantitative real-time PCR—Total RNA from mouse lymphatic ECs, HLECs or HUVECs was purified using Trizol (Invitrogen, Carlsbad, CA, USA) according to manufacturers instructions. cDNA was synthesized from total RNA (0.1 – 1.0 μg) with iScript Advanced cDNA Synthesis Kit (BioRad, Hercules, CA, USA). QRT-PCR was performed using PowerUp SYBR Green Master Mix reagent (Applied Biosystems, CA, USA) in a CFX96 Real-Time System (Bio-Rad, Hercules, CA, USA). Expression levels were normalized to *GAPDH*. Primer sequences are provided in the Table S1.

Scanning Electron Microscopy—SEM was performed according to our previous protocol (Geng et al., 2016). Embryos were fixed in 4% PFA overnight and vibratome sections were prepared to dissect the LVV-containing regions. The selected sections were fixed in 2% glutaraldehyde in 0.1 M cacodylate buffer for 2 hours. After washing profusely in PBS, the sections were post fixed in 1% osmium tetroxide in 0.1 M cacodylate buffer for 2 hours. Subsequently, the samples were dehydrated by sequentially washing in increasing concentrations of ethanol. The sections were further dehydrated in hexamethldisilazane (HMDS) and allowed to air-dry overnight. Dry sections were sputter-coated with Au/Pd particles (Med-010 Sputter Coater by Balzers-Union, USA) and observed under Quanta SEM (FEI, Hillsboro, OR, USA) at an accelerating voltage of 20KV.

Valve-Function Tests—LV leakiness and competence were quantified using recently described *ex vivo*, cannulated-vessel approach (Lapinski et al., 2017) (Figure S5K). Briefly, with the LV closed, the output pressure (P_{out}) determined by the output cannula was gradually increased (0.5 to 80 cm H_2O) while keeping the input pressure (P_{in}) constant. The internal pressure behind LVs is measured with a servo nulling micropipette (P_{sn}). Elevated P_{sn} implies LV leakiness. Starting with the valve open, P_{in} was held constant while P_{out} was gradually increased to determine when the LV closes. Dysfunctional valves require higher P_{out} to close.

QUANTIFICATION AND STATISTICAL ANALYSIS

For biochemical studies the number *n* refers to the number of times the experiment was performed. For histochemical analysis *n* refers to the total number of animals included per group. Statistically significant differences were determined using unpaired t test. Prism software was used for statistical analyses. Data are reported as mean ± SEM with significance set at $P < 0.05$. n and p values for each experiment is provided in the figure legends.

Supplementary Material

Refer to Web version on PubMed Central for supplementary material.

ACKNOWLEDGMENTS

We thank Dr. Angela Andersen (Life Science Editors) for editorial assistance, Mrs. Lisa Whitworth and Mr. Brent Johnson (Oklahoma State University) for scanning electron microscopy, and Dr. Jing Yang (University of Illinois, Urbana-Champaign) for insightful suggestions. This work is supported by NIH/ NHLBI (R01HL131652 to R.S.S. and T.H.K.; R01HL133216 to R.S.S., H.C., and J.B.D.; and R01HL122578 to M.J.D.), NIH/NICHH R01HD081534 (to B.J.M.), the Oklahoma Center for Adult Stem Cell Research, a program of TSET (4340 to R.S.S.), NIH/NIGMS COBRE (P20 GM103441 to X.G.; PI, Dr. McEver), the American Heart Association

(15BGIA25710032 to R.S.S.; 15POST25080182 to B.C.; and 16PRE31190025 to M.R.M.), and the National Research Foundation of Korea (NRF-2016R1E1A1A01943544 to E.-h.J.).

REFERENCES

Bazigou E, Xie S, Chen C, Weston A, Miura N, Sorokin L, Adams R, Muro AF, Sheppard D, and Makinen T (2009). Integrin-alpha9 is required for fibronectin matrix assembly during lymphatic valve morphogenesis. Dev. Cell 17, 175–186. [PubMed: 19686679]

Bixel MG, and Adams RH (2008). Master and commander: continued expression of Prox1 prevents the dedifferentiation of lymphatic endothelial cells. Genes Dev. 22, 3232–3235. [PubMed: 19056879]

Brault V, Moore R, Kutsch S, Ishibashi M, Rowitch DH, McMahon AP, Sommer L, Boussadia O, and Kemler R (2001). Inactivation of the beta-catenin gene by Wnt1-Cre-mediated deletion results in dramatic brain malformation and failure of craniofacial development. Development 128, 1253–1264. [PubMed: 11262227]

Carpenter AC, Rao S, Wells JM, Campbell K, and Lang RA (2010). Generation of mice with a conditional null allele for Wntless. Genesis 48, 554–558. [PubMed: 20614471]

Cha B, Kim W, Kim YK, Hwang BN, Park SY, Yoon JW, Park WS, Cho JW, Bedford MT, and Jho EH (2011). Methylation by protein arginine methyltransferase 1 increases stability of Axin, a negative regulator of Wnt signaling. Oncogene 30, 2379–2389. [PubMed: 21242974]

Cha B, Geng X, Mahamud MR, Fu J, Mukherjee A, Kim Y, Jho EH, Kim TH, Kahn ML, Xia L, et al. (2016). Mechanotransduction activates canonical Wnt/β-catenin signaling to promote lymphatic vascular patterning and the development of lymphatic and lymphovenous valves. Genes Dev. 30, 1454–1469. [PubMed: 27313318]

Choi D, Ramu S, Park E, Jung E, Yang S, Jung W, Choi I, Lee S, Kim KE, Seong YJ, et al. (2016). Aberrant Activation of Notch Signaling Inhibits PROX1 Activity to Enhance the Malignant Behavior of Thyroid Cancer Cells. Cancer Res. 76, 582–593. [PubMed: 26609053]

Choi D, Park E, Jung E, Seong YJ, Yoo J, Lee E, Hong M, Lee S, Ishida H, Burford J, et al. (2017). Laminar flow downregulates Notch activity to promote lymphatic sprouting. J. Clin. Invest 127, 1225–1240. [PubMed: 28263185]

Fiedler M, Graeb M, Mieszczanek J, Rutherford TJ, Johnson CM, and Bienz M (2015). An ancient Pygo-dependent Wnt enhanceosome integrated by Chip/LDB-SSDP. eLife 4.

Franco CA, Jones ML, Bernabeu MO, Vion AC, Barbacena P, Fan J, Mathivet T, Fonseca CG, Ragab A, Yamaguchi TP, et al. (2016). Non-canonical Wnt signalling modulates the endothelial shear stress flow sensor in vascular remodelling. eLife 5, e07727. [PubMed: 26845523]

Geng X, Cha B, Mahamud MR, Lim KC, Silasi-Mansat R, Uddin MKM, Miura N, Xia L, Simon AM, Engel JD, et al. (2016). Multiple mouse models of primary lymphedema exhibit distinct defects in lymphove-nous valve development. Dev. Biol 409, 218–233. [PubMed: 26542011]

Geng X, Cha B, Mahamud MR, and Srinivasan RS (2017). Intraluminal valves: development, function and disease. Dis. Model. Mech 10, 1273–1287. [PubMed: 29125824]

Gonsalves FC, Klein K, Carson BB, Katz S, Ekas LA, Evans S, Nagourney R, Cardozo T, Brown AM, and DasGupta R (2011). An RNAi-based chemical genetic screen identifies three small-molecule inhibitors of the Wnt/wingless signaling pathway. Proc. Natl. Acad. Sci. USA 108, 5954–5963. [PubMed: 21393571]

Harvey NL, Srinivasan RS, Dillard ME, Johnson NC, Witte MH, Boyd K, Sleeman MW, and Oliver G (2005). Lymphatic vascular defects promoted by Prox1 haploinsufficiency cause adult-onset obesity. Nat. Genet 37, 1072–1081. [PubMed: 16170315]

Holtwick R, Gotthardt M, Skryabin B, Steinmetz M, Potthast R, Zetsche B, Hammer RE, Herz J, and Kuhn M (2002). Smooth muscle-selective deletion of guanylyl cyclase-A prevents the acute but not chronic effects of ANP on blood pressure. Proc. Natl. Acad. Sci. USA 99, 7142–7147. [PubMed: 11997476]

Hong YK, and Detmar M (2003). Prox1, master regulator of the lymphatic vasculature phenotype. Cell Tissue Res. 314, 85–92. [PubMed: 12883994]

Janardhan HP, Milstone ZJ, Shin M, Lawson ND, Keaney JF, Jr., and Trivedi CM (2017). Hdac3 regulates lymphovenous and lymphatic valve formation. J. Clin. Invest 127, 4193–4206. [PubMed: 29035278]

Joeng KS, Schumacher CA, Zylstra-Diegel CR, Long F, and Williams BO (2011). Lrp5 and Lrp6 redundantly control skeletal development in the mouse embryo. Dev. Biol 359, 222–229. [PubMed: 21924256]

Johnson NC, Dillard ME, Baluk P, McDonald DM, Harvey NL, Frase SL, and Oliver G (2008). Lymphatic endothelial cell identity is reversible and its maintenance requires Prox1 activity. Genes Dev. 22, 3282–3291. [PubMed: 19056883]

Kabiri Z, Greicius G, Madan B, Biechele S, Zhong Z, Zaribafzadeh H, Edison, Aliyev J, Wu Y, Bunte R, et al. (2014). Stroma provides an intestinal stem cell niche in the absence of epithelial Wnts. Development 141, 2206–2215. [PubMed: 24821987]

Kanady JD, Munger SJ, Witte MH, and Simon AM (2015). Combining Foxc2 and Connexin37 deletions in mice leads to severe defects in lymphatic vascular growth and remodeling. Dev. Biol 405, 33–46. [PubMed: 26079578]

Kazenwadel J, Secker GA, Betterman KL, and Harvey NL (2012). In vitro assays using primary embryonic mouse lymphatic endothelial cells uncover key roles for FGFR1 signalling in lymphangiogenesis. PLoS ONE 7, e40497. [PubMed: 22792354]

Kazenwadel J, Betterman KL, Chong CE, Stokes PH, Lee YK, Secker GA, Agalarov Y, Demir CS, Lawrence DM, Sutton DL, et al. (2015). GATA2 is required for lymphatic vessel valve development and maintenance. J. Clin. Invest 125, 2979–2994. [PubMed: 26214525]

Kisanuki YY, Hammer RE, Miyazaki J, Williams SC, Richardson JA, and Yanagisawa M (2001). Tie2-Cre transgenic mice: a new model for endothelial cell-lineage analysis in vivo. Dev. Biol 230, 230–242. [PubMed: 11161575]

Koltowska K, Lagendijk AK, Pichol-Thievend C, Fischer JC, Francois M, Ober EA, Yap AS, and Hogan BM (2015). Vegfc Regulates Bipotential Precursor Division and Prox1 Expression to Promote Lymphatic Identity in Zebrafish. Cell Rep. 13, 1828–1841. [PubMed: 26655899]

Korinek V, Barker N, Morin PJ, van Wichen D, de Weger R, Kinzler KW, Vogelstein B, and Clevers H (1997). Constitutive transcriptional activation by a beta-catenin-Tcf complex in APC−/− colon carcinoma. Science 275, 1784–1787. [PubMed: 9065401]

Lapinski PE, Lubeck BA, Chen D, Doosti A, Zawieja SD, Davis MJ, and King PD (2017). RASA1 regulates the function of lymphatic vessel valves in mice. J. Clin. Invest 127, 2569–2585. [PubMed: 28530642]

Li R, Beebe T, Jen N, Yu F, Takabe W, Harrison M, Cao H, Lee J, Yang H, Han P, et al. (2014). Shear stress-activated Wnt-angiopoietin-2 signaling recapitulates vascular repair in zebrafish embryos. Arterioscler. Thromb. Vasc. Biol 34, 2268–2275. [PubMed: 25147335]

Liu J, Pan S, Hsieh MH, Ng N, Sun F, Wang T, Kasibhatla S, Schuller AG, Li AG, Cheng D, et al. (2013). Targeting Wnt-driven cancer through the inhibition of Porcupine by LGK974. Proc. Natl. Acad. Sci. USA 110, 20224–20229. [PubMed: 24277854]

Liu Y, Ye X, Zhang JB, Ouyang H, Shen Z, Wu Y, Wang W, Wu J, Tao S, Yang X, et al. (2015). PROX1 promotes hepatocellular carcinoma proliferation and sorafenib resistance by enhancing β-catenin expression and nuclear translocation. Oncogene 34, 5524–5535. [PubMed: 25684142]

Liu X, Uemura A, Fukushima Y, Yoshida Y, and Hirashima M (2016). Semaphorin 3G Provides a Repulsive Guidance Cue to Lymphatic Endothelial Cells via Neuropilin-2/PlexinD1. Cell Rep. 17, 2299–2311. [PubMed: 27880905]

Logan CY, and Nusse R (2004). The Wnt signaling pathway in development and disease. Annu. Rev. Cell Dev. Biol 20, 781–810. [PubMed: 15473860]

Machnik A, Neuhofer W, Jantsch J, Dahlmann A, Tammela T, Machura K, Park JK, Beck FX, Muüller DN, Derer W, et al. (2009). Macrophages regulate salt-dependent volume and blood pressure by a vascular endothelial growth factor-C-dependent buffering mechanism. Nat. Med 15, 545–552. [PubMed: 19412173]

Madisen L, Zwingman TA, Sunkin SM, Oh SW, Zariwala HA, Gu H, Ng LL, Palmiter RD, Hawrylycz MJ, Jones AR, et al. (2010). A robust and high-throughput Cre reporting and characterization system for the whole mouse brain. Nat. Neurosci 13, 133–140. [PubMed: 20023653]

Mao B, Wu W, Li Y, Hoppe D, Stannek P, Glinka A, and Niehrs C (2001). LDL-receptor-related protein 6 is a receptor for Dickkopf proteins. Nature 411, 321–325. [PubMed: 11357136]

Niehrs C, and Shen J (2010). Regulation of Lrp6 phosphorylation. Cell. Mol. Life Sci 67, 2551–2562. [PubMed: 20229235]

Norrme n, C., Ivanov KI, Cheng J, Zangger N, Delorenzi M, Jaquet M, Miura N, Puolakkainen P, Horsley V, Hu J, et al. (2009). FOXC2 controls formation and maturation of lymphatic collecting vessels through cooperation with NFATc1. J. Cell Biol 185, 439–457. [PubMed: 19398761]

Olson LE, Tollkuhn J, Scafoglio C, Krones A, Zhang J, Ohgi KA, Wu W, Taketo MM, Kemler R, Grosschedl R, et al. (2006). Homeodomainmediated beta-catenin-dependent switching events dictate cell-lineage determination. Cell 125, 593–605. [PubMed: 16678101]

Petrova TV, Ma¨ kinen T, Ma¨ kela¨ TP, Saarela J, Virtanen I, Ferrell RE, Finegold DN, Kerjaschki D, Yla¨ -Herttuala S, and Alitalo K (2002). Lymphatic endothelial reprogramming of vascular endothelial cells by the Prox-1 homeobox transcription factor. EMBO J. 21, 4593–4599. [PubMed: 12198161]

Petrova TV, Karpanen T, Norrme´ n C, Mellor R, Tamakoshi T, Finegold D, Ferrell R, Kerjaschki D, Mortimer P, Yla¨ -Herttuala S, et al. (2004). Defective valves and abnormal mural cell recruitment underlie lymphatic vascular failure in lymphedema distichiasis. Nat. Med 10, 974–981. [PubMed: 15322537]

Pham TH, Baluk P, Xu Y, Grigorova I, Bankovich AJ, Pappu R, Coughlin SR, McDonald DM, Schwab SR, and Cyster JG (2010). Lymphatic endothelial cell sphingosine kinase activity is required for lymphocyte egress and lymphatic patterning. J. Exp. Med 207, 17–27. [PubMed: 20026661]

Ptashne M (2007). On the use of the word 'epigenetic'. Curr. Biol 17, R233–R236. [PubMed: 17407749]

Qu Q, Sun G, Murai K, Ye P, Li W, Asuelime G, Cheung YT, and Shi Y (2013). Wnt7a regulates multiple steps of neurogenesis. Mol. Cell. Biol 33, 2551–2559. [PubMed: 23629626]

Railo A, Pajunen A, Ita¨ ranta P, Naillat F, Vuoristo J, Kilpela¨ inen P, and Vainio S (2009). Genomic response to Wnt signalling is highly context-dependent–evidence from DNA microarray and chromatin immunoprecipitation screens of Wnt/TCF targets. Exp. Cell Res 315, 2690–2704. [PubMed: 19563800]

Renier N, Wu Z, Simon DJ, Yang J, Ariel P, and Tessier-Lavigne M (2014). iDISCO: a simple, rapid method to immunolabel large tissue samples for volume imaging. Cell 159, 896–910. [PubMed: 25417164]

Ruocco V, Schwartz RA, and Ruocco E (2002). Lymphedema: an immunologically vulnerable site for development of neoplasms. J. Am. Acad. Dermatol 47, 124–127. [PubMed: 12077591]

Sabine A, Agalarov Y, Maby-El Hajjami H, Jaquet M, Ha¨ gerling R, Pollmann C, Bebber D, Pfenniger A, Miura N, Dormond O, et al. (2012). Mechanotransduction, PROX1, and FOXC2 cooperate to control connexin37 and calcineurin during lymphatic-valve formation. Dev. Cell 22, 430–445. [PubMed: 22306086]

Sato N, Meijer L, Skaltsounis L, Greengard P, and Brivanlou AH (2004). Maintenance of pluripotency in human and mouse embryonic stem cells through activation of Wnt signaling by a pharmacological GSK-3-specific inhibitor. Nat. Med 10, 55–63. [PubMed: 14702635]

Sato T, van Es JH, Snippert HJ, Stange DE, Vries RG, van den Born M, Barker N, Shroyer NF, van de Wetering M, and Clevers H (2011). Paneth cells constitute the niche for Lgr5 stem cells in intestinal crypts. Nature 469, 415–418. [PubMed: 21113151]

Schuijers J, Mokry M, Hatzis P, Cuppen E, and Clevers H (2014). Wntinduced transcriptional activation is exclusively mediated by TCF/LEF. EMBO J. 33, 146–156. [PubMed: 24413017]

Srinivasan RS, and Oliver G (2011). Prox1 dosage controls the number of lymphatic endothelial cell progenitors and the formation of the lymphovenous valves. Genes Dev. 25, 2187–2197. [PubMed: 22012621]

Srinivasan RS, Geng X, Yang Y, Wang Y, Mukatira S, Studer M, Porto MP, Lagutin O, and Oliver G (2010). The nuclear hormone receptor CoupTFII is required for the initiation and early maintenance of Prox1 expression in lymphatic endothelial cells. Genes Dev. 24, 696–707. [PubMed: 20360386]

Srinivasan RS, Escobedo N, Yang Y, Interiano A, Dillard ME, Finkelstein D, Mukatira S, Gil HJ, Nurmi H, Alitalo K, and Oliver G (2014). The Prox1-Vegfr3 feedback loop maintains the identity and the number of lymphatic endothelial cell progenitors. Genes Dev. 28, 2175–2187. [PubMed: 25274728]

Sustmann C, Flach H, Ebert H, Eastman Q, and Grosschedl R (2008). Cell-type-specific function of BCL9 involves a transcriptional activation domain that synergizes with beta-catenin. Mol. Cell. Biol 28, 3526–3537. [PubMed: 18347063]

Sweet DT, Jime´ nez JM, Chang J, Hess PR, Mericko-Ishizuka P, Fu J, Xia L, Davies PF, and Kahn ML (2015). Lymph flow regulates collecting lymphatic vessel maturation in vivo. J. Clin. Invest 125, 2995–3007. [PubMed: 26214523]

Tammela T, and Alitalo K (2010). Lymphangiogenesis: Molecular mechanisms and future promise. Cell 140, 460–476. [PubMed: 20178740]

Tatin F, Taddei A, Weston A, Fuchs E, Devenport D, Tissir F, and Makinen T (2013). Planar cell polarity protein Celsr1 regulates endothelial adherens junctions and directed cell rearrangements during valve morphogenesis. Dev. Cell 26, 31–44. [PubMed: 23792146]

Turner CJ, Badu-Nkansah K, Crowley D, van der Flier A, and Hynes RO (2014). Integrin-a5b1 is not required for mural cell functions during development of blood vessels but is required for lymphatic-blood vessel separation and lymphovenous valve formation. Dev. Biol 392, 381–392. [PubMed: 24858485]

Vermot J, Forouhar AS, Liebling M, Wu D, Plummer D, Gharib M, and Fraser SE (2009). Reversing blood flows act through klf2a to ensure normal valvulogenesis in the developing heart. PLoS Biol. 7, e1000246. [PubMed: 19924233]

Wong BW, Wang X, Zecchin A, Thienpont B, Cornelissen I, Kalucka J, García-Caballero M, Missiaen R, Huang H, Bru€ning U, et al. (2017). The role of fatty acid β-oxidation in lymphangiogenesis. Nature 542, 49–54. [PubMed: 28024299]

Wu CI, Hoffman JA, Shy BR, Ford EM, Fuchs E, Nguyen H, and Merrill BJ (2012). Function of Wnt/β-catenin in counteracting Tcf3 repression through the Tcf3-β-catenin interaction. Development 139, 2118–2129. [PubMed: 22573616]

Yoshimatsu Y, Yamazaki T, Mihira H, Itoh T, Suehiro J, Yuki K, Harada K, Morikawa M, Iwata C, Minami T, et al. (2011). Ets family members induce lymphangiogenesis through physical and functional interaction with Prox1. J. Cell Sci 124, 2753–2762. [PubMed: 21807940]

Highlights

- Wnt ligands from two cell types regulate lymphatic vascular development
- Oscillatory shear stress stimulates autocrine Wnt/β-catenin signaling d Smooth muscle cells are an additional source of Wnt ligands
- PROX1 interacts with β-catenin and TCF7L1 to regulate Wnt/β-catenin signaling

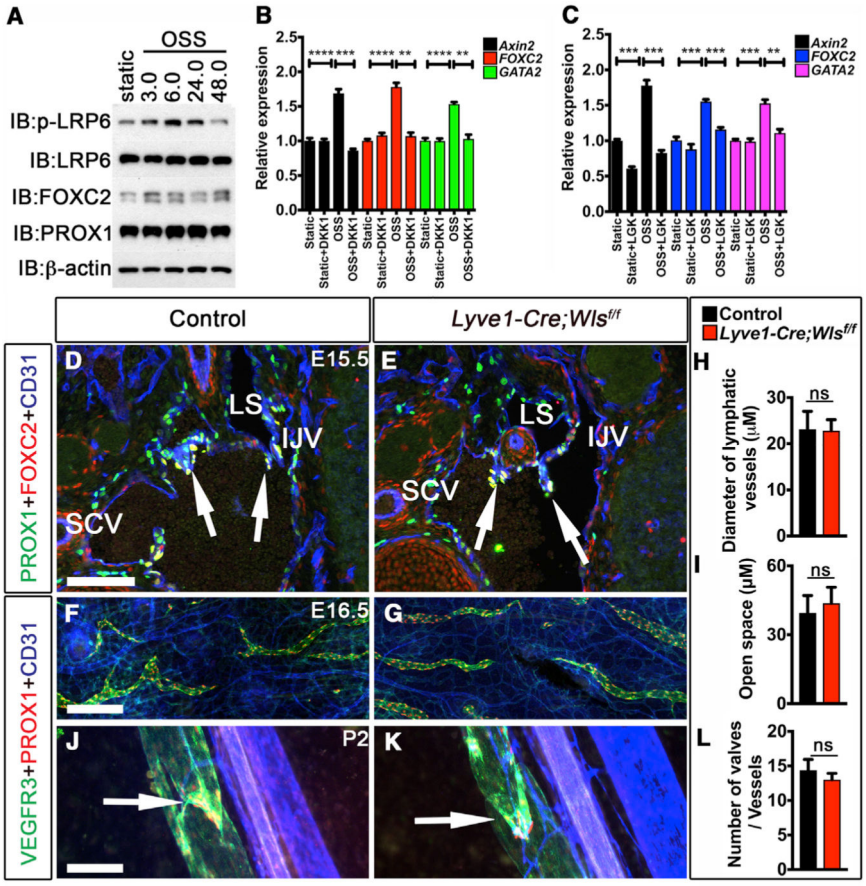

Figure 1. Autocrine Wnt/β-Catenin Signaling Is Activated in HLECs byOSS *In Vitro*, but It Is Dispensable for Lymphatic Vascular Development *In Vivo*

(A) HLECs were exposed to oscillatory shear stress (OSS) for the indicated number of hours. Subsequently, the cells were harvested and analyzed by western blotting using the indicated antibodies. Phosphorylation of LRP6 is increased by OSS.

(B and C) HLECs were cultured under OSS with recombinant DKK1, which inhibits the interaction between Wnt ligands and LRP co-receptors (B), or LGK-974, which inhibits the secretion of Wnt ligands from cells (C). Subsequently, RNA was extracted, and the expression of *AXIN2*, *FOXC2*, and *GATA2* was evaluated by real-time qPCR analysis. The data were normalized to *GAPDH*. Both DKK1 and LGK-974 inhibit OSS-induced expression of *AXIN2, FOXC2*, and *GATA2*.

(D and E) E15.5 LVVs are observed in both *Lyve1Cre*;*Wls*$^{f/f}$ (E) and control (D) littermate embryos (arrows).

(F–I) Whole-mount immunohistochemistry on the dorsal skin of E16.5 wild-type (F) and *Lyve1Cre;Wls*$^{f/f}$ (G) embryos reveals normal lymphatic vessels. The diameters of lymphatic vessels (H) and their migration toward the dorsal midline (I) are not different between E17.5 control and mutant embryos.

(J–L)Normal-looking LVs are observed inmesenteric lymphatic vessels of P2 control (J, arrow) and *Lyve1Cre;Wls*$^{f/f}$ mice (K,arrow). The number of E18.5 LVs is not changed in *Lyve1-Cre;Wls*$^{f/f}$ mice (L).

LVV, lymphovenous valve; LV, lymphatic valve;IJV, internal jugular vein; SCV, subclavian vein. Scale bars, 100 mm (D–G) and 200 mm (J and K). Statistics: (A)–(C), n = 3; (D)–(L), n = 4 per genotype per stage; **p < 0.01, ***p < 0.001, ****p < 0.0001. Error bars in graphs represent ± SEM.

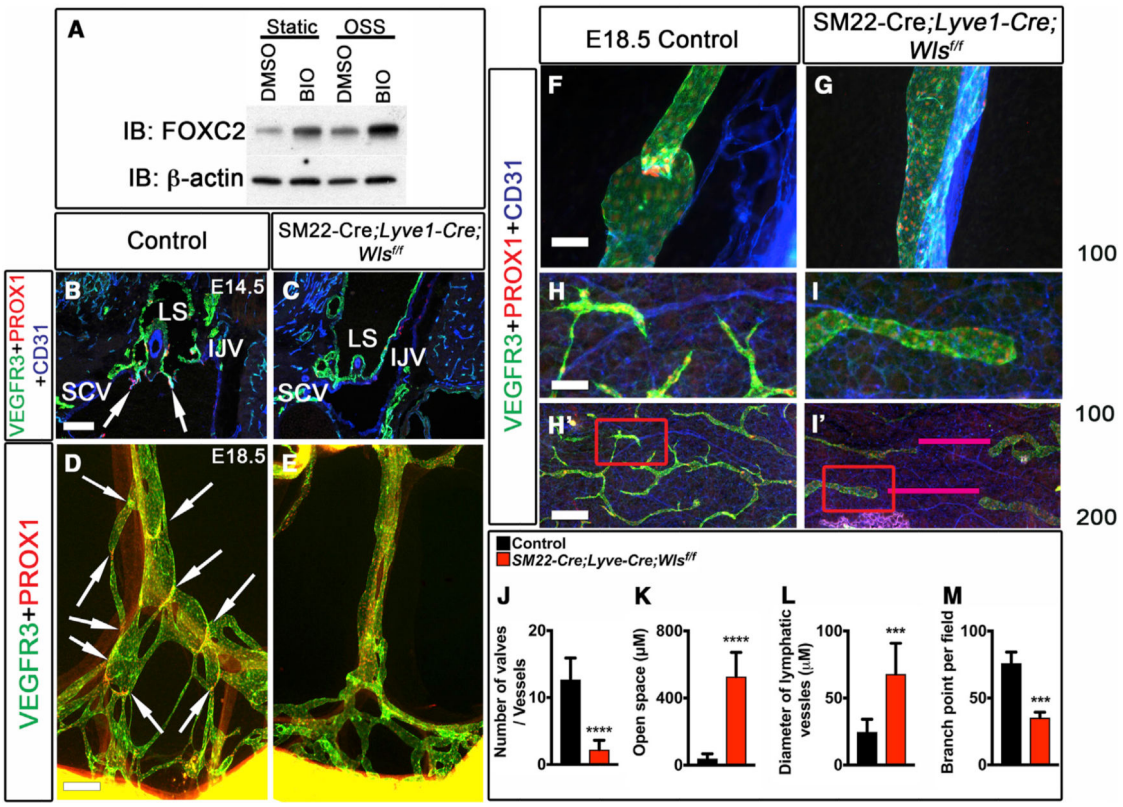

Figure 2. LEC- and Vascular Smooth Muscle Cell-Derived Wnt Ligands Play Complementary Roles during Lymphatic Vascular Development

(A) HLECs were cultured under OSS with or without the Wnt agonist BIO. Subsequently, cells were lysed, and western blot was performed for the indicated molecules. Both OSS and BIO enhance FOXC2 expression. BIO enhances FOXC2 expression to a greater extent compared with OSS. Additionally, a much stronger expression of FOXC2 is observed in HLECs cultured with both OSS and BIO.

(B–I) *W/s* was simultaneously deleted from LECs and vascular smooth muscle cells by *Lyve1-Cre* and SM22-Cre. The control and mutant embryos were harvested at the indicated developmental time points and analyzed by immunohistochemistry on frontal cryosections (B and C) or by whole-mount immunohistochemistry(D–I).

(B and C) LVVs are observed at the junction of lymph sacs (LSs), IJV, and subclavian vein (SCV) in control (B, arrows) but not in SM22-Cre;*Lyve1-Cre;W/s*$^{f/f}$ embryos (C).

(D–G) LVs are observed in the mesenteric lymphatic vessels of control embryos (D, arrows, and F). LVs are mostly absent from the mesenteric lymphatic vessels of SM22-Cre;*Lyve1-Cre;W/s*$^{f/f}$ embryos (E and G).

(H–I´) (H) and (I) are higher-magnification images of the boxed areas in (H´) and (I´), respectively. The lymphatic vessels of the dorsal skin are dilated in mutant embryos. The distance between the opposing migrating fronts is higher in SM22-Cre;*Lyve1-Cre;W/s*$^{f/f}$ embryos (magenta bars in I'). Additionally, fewer branchpoints are observed in the lymphatic vessels of mutant embryos.

(J–M) The number of mesenteric LVs per lymphatic vessel is quantified in (J). The lymphatic vessels of the dorsal skin were analyzed, and the distance between the migrating

fronts (K), diameters of lymphatic vessels (L), and the number of branchpoints (M) were quantified.

Scale bars, 100 mM (B, C, and F–I), 200 mM (H' and I'), and 250 mM (D and E). Statistics: (A), n = 3; (B)–(M), n = 4 per genotype; ***p < 0.001, ****p < 0.0001. Error bars in graphs represent ± SEM.

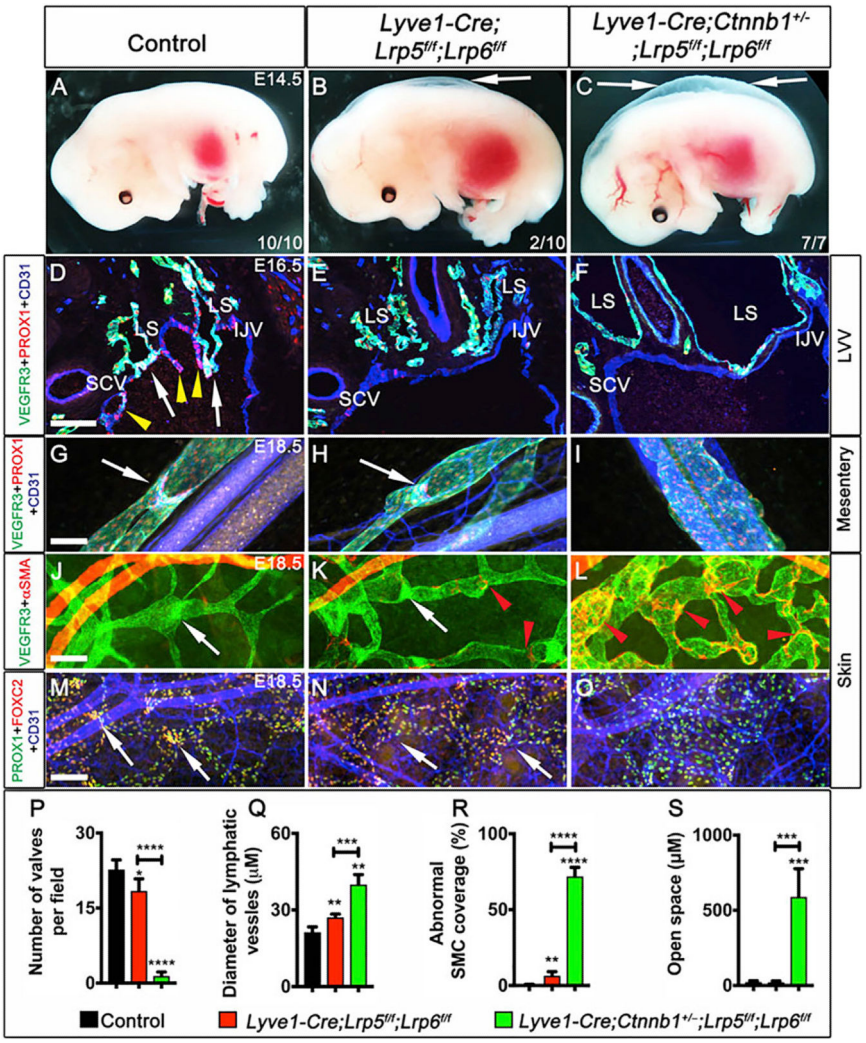

Figure 3. Wnt/β-Catenin Signaling via LRP5/ 6 Is Necessary for Lymphatic Vascular Development

(A–C) E14.5 control embryos do not display edema (A). A subset of E14.5 *Lyve1-Cre;Lrp5$^{f/f}$; Lrp6$^{f/f}$* (B) and all of the E14.5 *Lyve1-Cre; Ctnnb1$^{+/}$;Lrp5$^{f/f}$;Lrp6$^{f/f}$* (C) embryos display edema (arrows).

(D–F) LVVs (arrows) and VVs (yellow arrowheads) are observed at the junction of the IJV, SCV, and LSs in immunostained frontal cryosections of wildtype embryos (D). However, LVVs and VVs are not observed in *Lyve1-Cre;Lrp5$^{f/f}$;Lrp6$^{f/f}$* (E) or *Lyve1Cre;Ctnnb1$^{+/}$;Lrp5$^{f/f}$;Lrp6$^{f/f}$* embryos (F).

(G–O) LVs are present in mesenteric lymphatic vessels of wild-type and *Lyve1-Cre;Lrp5$^{f/f}$;Lrp6$^{f/f}$* embryos (G and H, arrows). However, LVs are absent in dysplastic mesenteric lymphatic vessels of *Lyve1-Cre;Ctnnb1$^{+/}$;Lrp5$^{f/f}$;Lrp6$^{f/f}$* embryos (I). LVs are present in the dorsal skin of wild-type (J and M, arrows) and *Lyve1-Cre;Lrp5$^{f/f}$;Lrp6$^{f/f}$* embryos (K and N, arrows). A few αSMA^{+} mural cells are abnormally recruited to the lymphatic vessels of *Lyve1-Cre;Lrp5$^{f/f}$;Lrp6$^{f/f}$* embryos (K, red arrowheads). LVs are absent in the dilated lymphatic vessels of *Lyve1-Cre;Ctnnb1$^{+/}$;Lrp5$^{f/f}$;Lrp6$^{f/f}$* embryos (L and O). Additionally, a profound increase in the amount of vascular smooth muscle cell recruitment

is observed (L, red arrowheads). (P–S) The number of LVs (P), lymphatic vessel diameter (Q), vascular smooth muscle cell (SMC) coverage (R), and open space between the migrating fronts (S) are quantified.

Scale bars, 100 mM. Statistics: In (A)–(C), the number of embryos analyzed and the number of embryos that are similar to the represented image are indicated in the bottom right corner. (D)–(S), n = 4 for each genotype; *$p < 0.05$, **$p < 0.005$, ***$p < 0.001$, ****$p < 0.0001$. Error bars in graphs represent ± SEM.

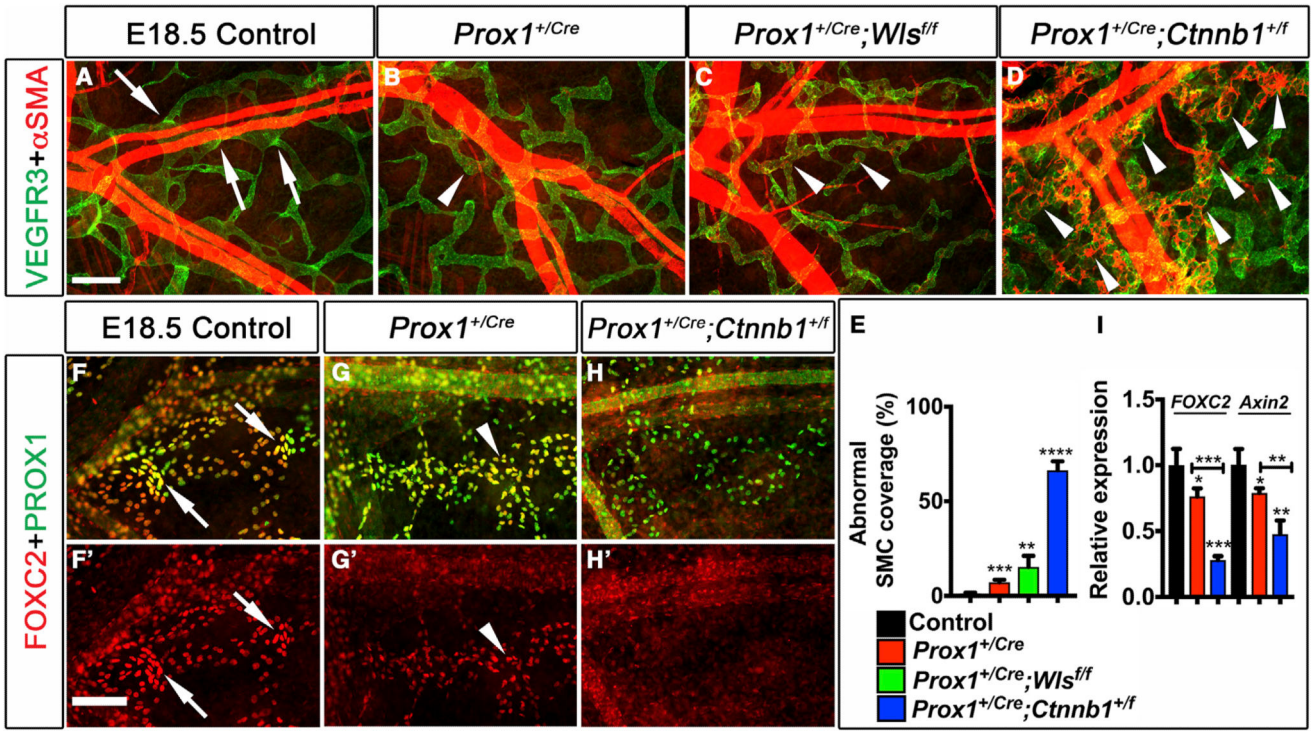

Figure 4. Prox1 Genetically Interacts with Autocrine and Paracrine Wnt/β-Catenin Signaling in Lymphatic Vascular Development

The lymphatic vessels in the dorsal skin of E18.5 wild-type, *Prox1*$^{+/Cre}$, *Prox1*$^{+/Cre}$;*W/s*$^{f/f}$, *and Prox1*$^{+/Cre}$; *Ctnnb1*$^{+/f}$ embryos were analyzed by whole-mount immunohistochemistry using the indicated antibodies.

(A–D) The lymphatic capillaries in the dorsal skin of control embryos (A) are devoid of αSMA^{+} vascular SMCs. A few SMCs are observed in the lymphatic capillaries of *Prox1*$^{+/Cre}$ (B) and *Prox1*$^{+/Cre}$;*W/s*$^{f/f}$ (C) embryos (arrowheads). (D) A dramatic increase in SMC coverage is observed in the lymphatic capillaries of *Prox1*$^{+/Cre}$;*Ctnnb1*$^{+/f}$ embryos (arrowhead).

(E) Quantification of SMC coverage in the lymphatic capillaries of various embryos.

(F–H') FOXC2 expression is downregulated in the LECs of *Prox1/Ctnnb1* double-heterozygous mice. In control embryos, PROX1^{high}; FOXC2^{high} LVs are clearly visible (F and F', arrows). Fewer LVs and downregulated FOXC2 expression are observed in *Prox1*$^{+/Cre}$ embryos (G and G', arrowhead). A more dramatic downregulation of FOXC2 expression is observed in the LECs of *Prox1*$^{+/Cre}$;*Ctnnb1*$^{+/f}$ embryos (H and H').

(I) LECs were isolated from the dorsal skin of E17.5 embryos. RNA was isolated, and real-time qPCR was performed for *Foxc2* and *Axin2*.

Scale bars, 200 mM (A–D) and 100 mM (F–H). Statistics: (A)–(H), n = 4 per genotype; (I), n = 3. *p < 0.05, **p < 0.01, ***p < 0.001, ****p < 0.0001. Error bars in graphs represent ± SEM.

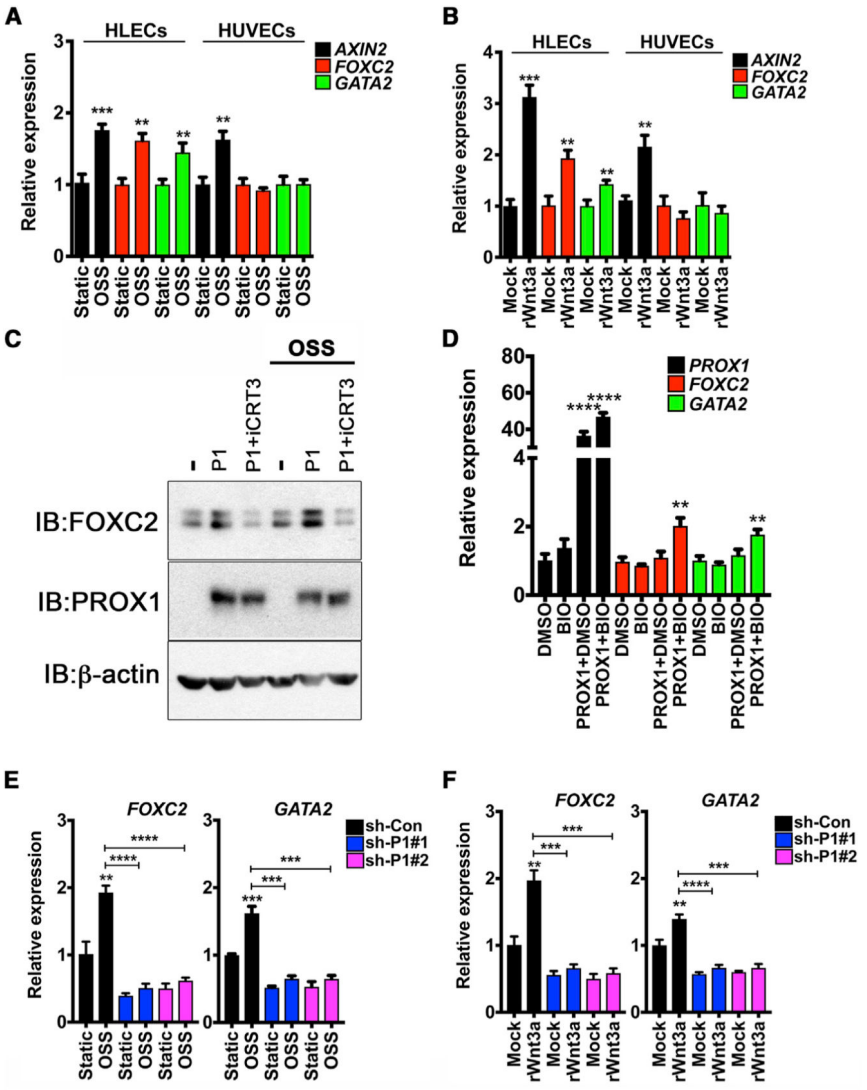

Figure 5. PROX1 Synergizes with Wnt/β-Catenin Signaling to Enhance GATA2 and FOXC2 Expression

(A and B) OSS and Wnt/β-catenin signaling do not enhance FOXC2 and GATA2 expression in human umbilical vein endothelial cells (HUVECs). Primary human lymphatic endothelial cells (HLECs) or HUVECs were cultured under OSS for 48 hr (A) or in the presence of recombinant Wnt3a (rWnt3a) for 24 hr (B). Subsequently, RNA was extracted and analyzed by real-time qPCR for *AXIN2, FOXC2*, and *GATA2*. The expression levels were normalized to that of GAPDH.

(C and D) PROX1 provides competence to HUVECs to respond to OSS and Wnt/β-catenin signaling and enhance the expression of FOXC2 and GATA2. HUVECs were infected with lentiviral particles expressing GFP or human PROX1 for 48 hr. Subsequently, the cells were exposed to (C) OSS for 48 hr or to (D) the Wnt agonist BIO for 12 hr.

(C) PROX1-expressing HUVECs were cultured under static or OSS conditions with or without the Wnt antagonist iCRT3. Western blot was performed to quantify FOXC2

expression. (D) PROX1-expressing HUVECs were cultured with BIO or DMSO for 24 hr, and the expression of *FOXC2* and *GATA2* was quantified by real-time qPCR.
(E and F) PROX1 is necessary for OSS- and Wnt/β-catenin signaling-mediated expression of FOXC2 and GATA2 in HLECs. HLECs were infected with lentiviral particles expressing shRNAs that target GFP (sh-Con) or PROX1 (sh-P1#1 and sh-P1#2) for 48 hr. Subsequently, HLECs were additionally cultured under OSS for 48 hr (E) or with rWnt3a for 24 hr (F). Real-time qPCR was performed to quantify the expression of *FOXC2* and *GATA2*.
Statistics: n = 3 for all experiments. **p < 0.01, ***p < 0.001, ****p < 0.0001. Error bars in graphs represent ± SEM.

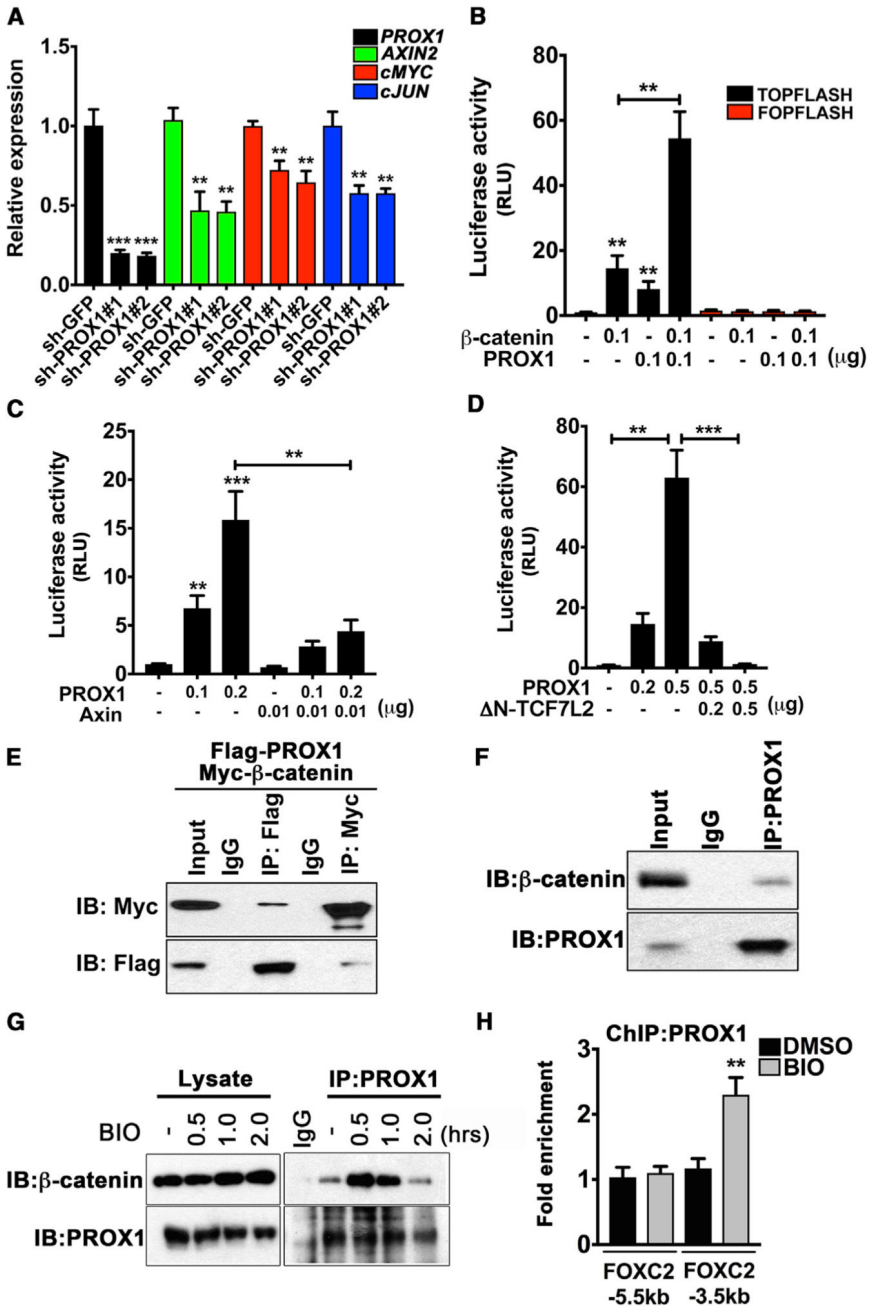

Figure 6. PROX1 Physically Interacts with β-Catenin and Enhances Wnt/β-Catenin Signaling

(A) PROX1 enhances the expression of Wnt/β-catenin signaling target genes in HLECs. HLECs were infected with lentiviral particles expressing shRNAs that target GFP (sh-GFP) or PROX1 (shPROX1#1 and sh-PROX1#2) for 72 hr. Subsequently, RNA was extracted, and real-time qPCR was performed for the expression of Wnt/β-catenin target genes.

(B–D) PROX1 synergizes with β-catenin to enhance Wnt/β-catenin signaling.

(B) 293T cells were co-transfected with TOPFlashor FOPFlash luciferase reporters with PROX1- and or β-catenin-expressing vectors. The TCF/LEF binding sites of TOPFLASH are inactivated to generate FOPFlash as a negative control for Wnt/β-catenin signaling.

(C and D) 293T cells were co-transfected with TOPFlash- and PROX1-expressing vectors together with AXIN-expressing (C) or ΔN-TCF7L2expressing (D) plasmids. DN-TCF7L2 cannot interact with β-catenin and functions as a dominant-negative mutant. A Renilla luciferase-expressing plasmid was used as an internal control, and luciferase activities were measured 36 hr after transfection.

(E–G) PROX1 associates with β-catenin.

(E) 293T cells were transfected with Myc-tagged β-catenin and FLAG-tagged PROX1 plasmids. 48 hr later, the cell lysate was subjected to a co-immunoprecipitation assay using anti-FLAG antibody or anti-Myc antibody. The precipitates were probed by western blot using the indicated antibodies.

(F) HLEC lysate was immunoprecipitated using anti-PROX1 antibody and probed by western blot using anti-PROX1 or anti-β-catenin antibodies. (G) HLECs were treated with BIO for the indicated number of hours. The lysates were analyzed as in (F).

(H) HLECs were treated with DMSO or BIO (0.5 μM) for 3 hr, and ChIP was performed using anti-PROX1 antibody. qPCR was performed using primers flanking the TCF/LEF-binding site in the 3.5 kb location. As a negative control, primers flanking a TCF/LEF-binding site that is located at a more upstream location (5.5 kb) were used.

Statistics: n = 3 for all experiments. **$p < 0.01$, ***$p < 0.001$. Error bars in graphs represent ± SEM.

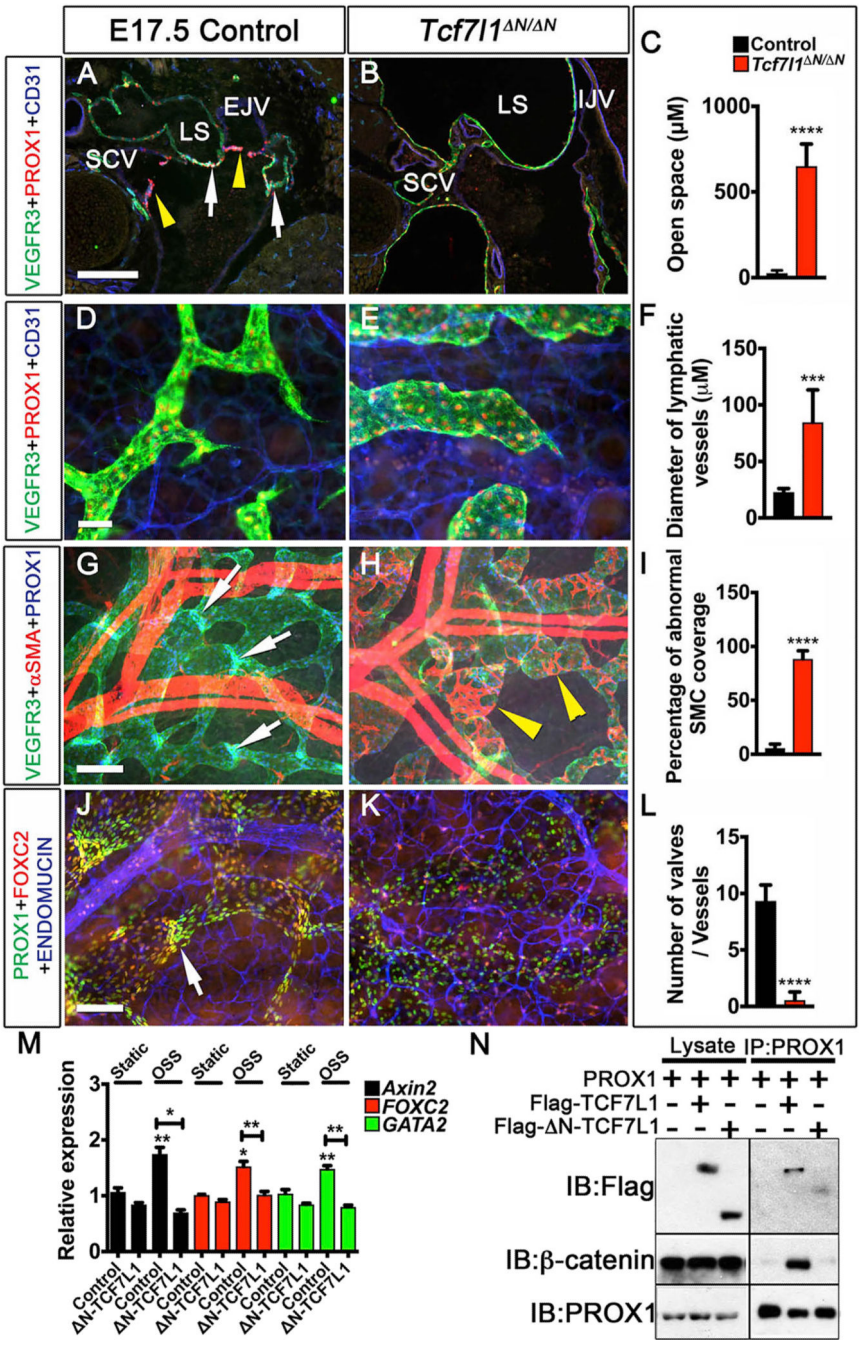

Figure 7. TCF7L1/β-Catenin Interaction Is Important for Lymphatic Vascular Development

(A and B) E17.5 embryos were frontally sectioned and analyzed using the indicated antibodies. Lymphovenous valves (arrows) and venous valves (yellow arrowheads) are present at the junction of the IJV, external jugular vein (EJV), SCV, and LSs of control (A) but not Tcf7l1$^{DN/DN}$ (B) embryos. (C–K) The dorsal skin of E17.5 embryos was analyzed by whole-mount immunohistochemistry. (C) The distance between the lymphatic vessel migrating fronts is significantly increased in *Tcf7l1*$^{\Delta N/\Delta N}$ embryos. A representative image is shown in Figure S6D.

(D–K) Compared to controls (D, G, and J), the lymphatic vessels of *Tcf7l1*$^{\Delta N/\Delta N}$ are dilated (E and F) and have abnormal αSMA^{+} vascular SMC coverage (H, yellow arrowheads, and I). PROX1^{high}; FOXC2^{high} LVs are observed in wild-type (G and J, arrows) but not in *Tcf7l1*$^{\Delta N/\Delta N}$ embryos (K).

LVs are rarely observed in the mesenteric lymphatic vessels of E17.5 *Tcf7l1*$^{\Delta N/\Delta N}$ embryos. Representative images are shown in Figures S6F and S6H.

(M) HLECs were infected with lentiviral particles expressing GFP or human ΔN-TCF7L1 for 24 hr. ΔN-TCF7L1 cannot interact with α-catenin and functions as a dominant-negative mutant. Subsequently, the cells were exposed to OSS for 48 hr, and the expression of *Axin2, FOXC2,* and *GATA2* was measured by real-time qPCR.

(N) 293T cells were transfected with PROX1 together with FLAG-tagged TCF7L1 or ΔNTCF7L1 plasmids. After 48 hr, an immunoprecipitation assay was performed using anti-PROX1 antibody. The precipitate was probed by western blot using the indicated antibodies to determine the interaction between PROX1, TCF7L1, and endogenous β-catenin. PROX1 interacts with TCF7L1 but not ΔN- TCF7L1. Furthermore, TCF7L1, but not ΔN-TCF7L1, enhances the interaction between PROX1 and β-catenin.

Scale bars, 200 μM (A, B, G, and H), 100 μM (J and K), and 50 μmM (D and E). Statistics: (A)–(L), n = 4 per genotype; (M) and (N), n = 3; *p < 0.05, **p < 0.01, ***p < 0.001, ****p < 0.0001. Error bars in graphs represent ± SEM.